NJC

Accepted Manuscript

This article can be cited before page numbers have been issued, to do this please use: A. O. Eseola, H. Görls, M. Bangesh and W. Plass, *New J. Chem.*, 2018, DOI: 10.1039/C8NJ01265B.

ROYAL SOCIETY OF CHEMISTRY

rsc.li/njc

View Article Online
DOI: 10.1039/C8NJ01265B

ESIPT-capable 2,6-di(1H-imidazol-2-yl)phenols with very strong fluorescent sensing signals towards Cr(III), Zn(II) and Cd(II): molecular variation effects on turn-on efficiency

Abiodun O. Eseola,[§,‡,*] Helmar Görls,[‡] Masroor Bangesh,[†] Winfried Plass,[‡,*]

[§]Materials Chemistry group, Department of Chemical Sciences, Redeemer's University Ede, Osun State, Nigeria.

[‡]Institut für Anorganische und Analytische Chemie, Friedrich-Schiller-Universität Jena, Humboldtstr. 8, D-07743 Jena, Germany.

[†]Department of Chemistry, Hazara University, Mansehra (Khyber Pakhtunkhwa) Pakistan.

Abstract

A series of structurally and electronically varied 2,6-di(1H-imidazol-2-yl)phenols that are ESIPT-capable (**1**–**12**) as well as the ESIPT-incapable 4,5-diphenyl-2-(3-(4,5-diphenyl-1H-imidazol-2-yl)phenyl)-1H-imidazole (**13**) have been designed and comparatively studied for molecular effects on sensitivity and selectivity characteristics as fluorescent chemosensors of

* Corresponding authors: Dr. A. O. Eseola: Materials Chemistry group, Department of Chemical Sciences, Redeemer's University Ede, Osun State, Nigeria; Tel.: +49(0)15218016407, +493641948138. e-mail: bioduneseola@hotmail.com; biodun.eseola@uni-jena.de; Prof. Dr. W. Plass; Address – Institut für Anorganische und Analytische Chemie, Friedrich-Schiller-Universität Jena, Humboldtstr. 8, D-07743 Jena, Germany; Tel.: +49 3641 948130; Fax: +49 3641948132; e-mail: sekr.plass@uni-jena.de

Electronic Supplementary Information (ESI) containing some further details is provided.

View Article Online
DOI: 10.1039/C8NJ01265B

Cr^{3+}, Zn^{2+} and Cd^{2+}. Single crystal structures revealed desired chain of intramolecular hydrogen bonding (ligand **12**) as well as possible coordination modes. Probes **1** – **4** demonstrated very high turn-on sensitivity and selectivity as double fluorescent sensors for Cr^{3+} and Zn^{2+} at their different emission wavelengths (blue-shifted in case of Zn^{2+}). A remarkable106-fold emission turn-on by Cr^{3+} was recorded for molecule **2**, which is an unknown magnitude for Cr^{3+} sensitivity to the best of our knowledge. Results revealed that Cd^{2+} sensor may be developed by further derivatization of these probes. Possession of symmetrical substitution on both imidazole rings, multiple active protons involved in hydrogen intramolecular bonding relay and the consequent ESIPT capability were found to be very beneficial to successful outcomes as high fluorescent turn-on chemosensors by the studied molecules. Modification of sensor properties such as sensitivity and selectivity was achieved through substituent manipulations at certain peripheral positions. Thus, deliberate molecular derivatization was found to be a tool for manipulating interference and selectivity profiles. Job plot, single crystal result and sustained large Stoke's shift in the presence of Cr^{3+} suggest a one-pocket N^O coordination in 1:1 stoichiometry rather than binuclear N^O^N two-pocket coordination. Quantum mechanical calculations on model structures suggest that successful turn-on results may be associated with coplanarity settings of the imidazole and phenol rings.

Keywords: Fluorescent chemosensors; Structure-Property-Correlation; ESIPT; Sustainable environment; Chromium(III), Zinc(II) and Cadmium(II)

1. Introduction

View Article Online
DOI: 10.1039/C8NJ01265B

Development of fluorescent chemosensors for environmentally and biologically important metal ions has remained an active area research.[1,2,3] Fluorescent chemosensors provide defined responses in the form of visible or analytically measurable signals. For metal ion sensing, such signals often depend on coordination interactions between target metal ions and a receptor site of appropriately configured heteroaromatic material.[4] Regardless of the classification as environmental or biological sensor (i.e. applicable for living cells), qualities like molecular stability, sensitivity and selectivity towards a target analyte are indispensable.[1,2,5]

Fluorescent sensing is attractive for its fast, simple and sensitive detection capabilities. Consequently, contributions from studies on various materials ranging from small molecules through polymeric substances to electrode-grafted molecules and nano-materials have continue to be documented.[6] However, small and well-characterized molecules are particularly valuable for uncovering structure-property correlations. For small molecular fluorophores, properties like geometry, steric features, coordination or donor strengths, composition, quantitative details, etc., are both easier to determine as well as to manipulate unlike for such species as surface-grafted or polymer materials. Consequently, small-molecule candidates should be chosen in order to explore underlying phenomena that supports efficient sensing characteristics.[7]

A reality however is that research contributions on metal ion fluorescent detection often involve only one or very few molecular analogues. As a result, knowledge of tolerance to derivatization or substituent effects is often unavailable for most reported sensor materials.[8,9] Several strange conclusions in literature about sensor coordination interactions can be attributed to inadequate understanding of the investigated molecules, which might be overcome by also examining more closely related analogues. In a typical example,[10] very uncommon imidazole

View Article Online
DOI: 10.1039/C8NJ01265B

deprotonation before coordination, very rare thiophene ring sulphur coordination[11] and a resultant chromium(II) product was proposed (Scheme 1 (a), compound ***IV***).

Deliberate derivatization of a sensor candidate may provide access to more details about the sensing action, create avenue for new sensor discoveries, allow incorporation of beneficial properties, enable modification of properties like solubility, cytotoxicity, sensitivity, selectivity, stability, etc.[12] For instance, excited state intramolecular proton-electron transfer (ESIPT, Scheme 1(b)) is known to improve accuracy of fluorescent sensing through the large Stoke-shifts that in turn prevent self-absorption.[13] ESIPT capability in fluorophore can be achieved by positioning an active proton in the proximity of a base donor.[9,14]

Chromium is the twenty-second most abundant elements of the earth crust and chromium in the environment results from industrial activities relating to production of synthetic ruby, leather processing, mordant dye of textile industry, alloy production, paints manufacture, application of the high-melting Cr_2O_3 for refractory materials, etc.[15] Despite the long standing discussion on chromium(III) ions as the so-called glucose tolerance factor (GTF), the current state of the art clearly indicates that chromium is not an essential element for mammals.[16] Moreover, above-normal chromium(III) concentrations in biological systems has been associated with damage to cellular structures.[17] Reported fluorescent sensors for chromium(III) are few and of generally weak to moderate turn-on capacity (Scheme 1 (a)).[10,18–23] The situation is different for zinc, as it is an essential trace element in the human body and enjoys substantial research attention in terms of analytical detection and medicinal applications.[24] Cadmium is however an established toxicant with severe health implications.[25] Albeit these biological differences, there is a great deal of interest in the detection of these metals.

View Article Online
DOI: 10.1039/C8NJ01265B

In our recent spectroscopic studies of donor strengths and ESIPT characteristics involving 4-methyl-2,6-bis(4,5-diphenyl-1H-imidazol-2-yl)phenol (compound **1**, Scheme 2)[26] and 2-(4,5-diphenyl-1H-imidazol-2-yl)phenol analogues,[27] hints for the metal ion sensing potential by these ligands were observed. Furthermore, the ligands alone in solvents possess low quantum yields, which is desirable for fluorescence turn-on. Therefore, with additional motivation from our previous experiences in the area of tuning steric and electronic properties of azole containing ligand frameworks,[28,29,30] the current study is aimed at examining metal ion sensing of some new fluorophores as well as to pursue possible understanding on the influence of structural and electronic variation on fluorescent turn-on behaviours. We herein present results for chemosensor investigations on several new 2-(1H-imidazol-2-yl)phenol dye analogues (Scheme 2).

View Article Online
DOI: 10.1039/C8NJ01265B

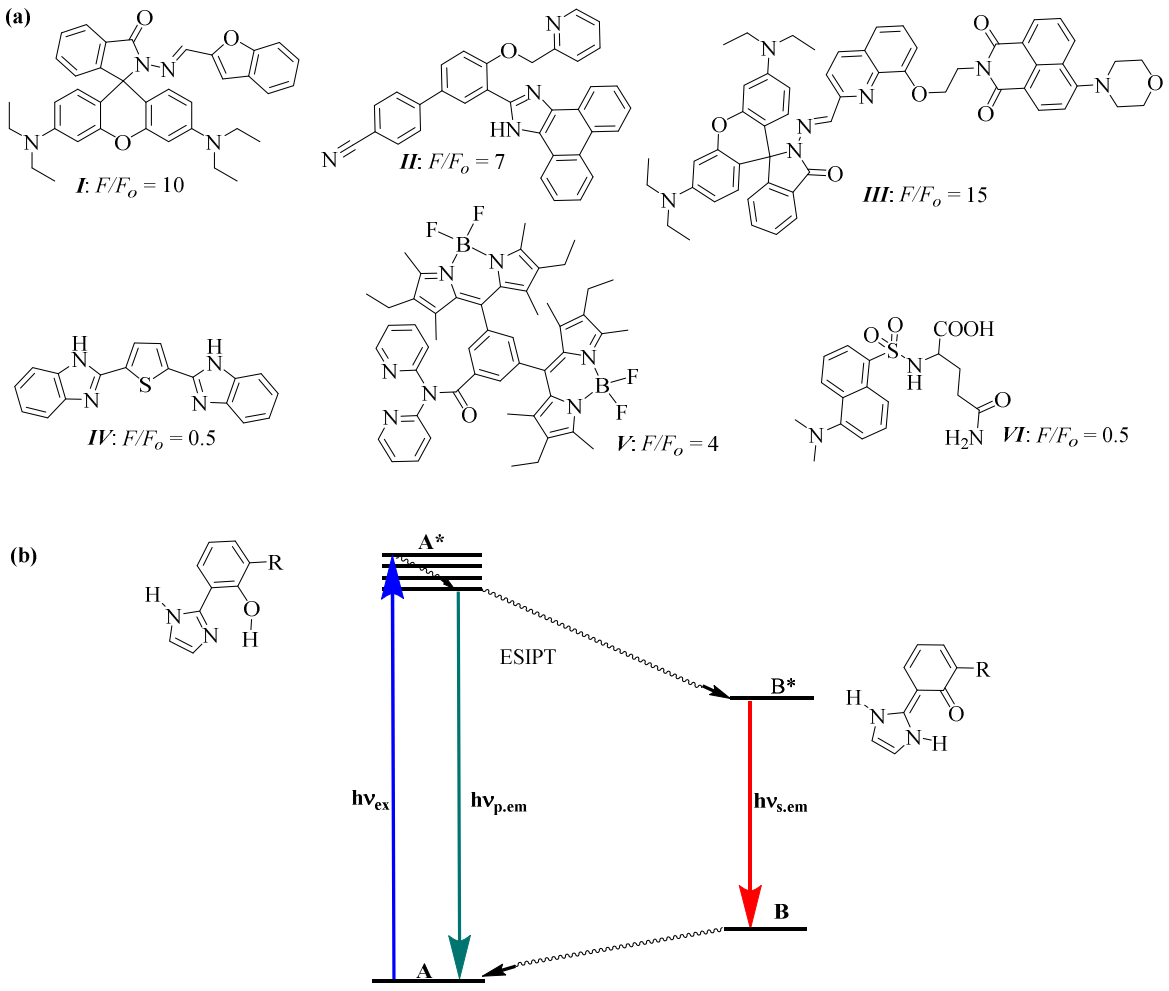

Scheme 1: **(a)** Various reported fluorescent probes for chromium(III) and their turn-on F/F_o magnitudes: ***I***,[18] ***II***,[19] ***III***,[20,21] ***IV***,[10] ***V***[22] and ***VI***.[23] (F and F_o are fluorescence intensity in the presence and absence of Cr^{3+} ion respectively). **(b)** Schematic illustration of the origin of large Stoke's shift in ESIPT emission: $h\nu_{ex}$ is excitation light, $h\nu_{p.em}$ is light emission from primary excited state (**A*→A**), $h\nu_{s.em}$ is Stoke's red-shifted light emission from secondary excited state (**B*→B**).

View Article Online
DOI: 10.1039/C8NJ01265B

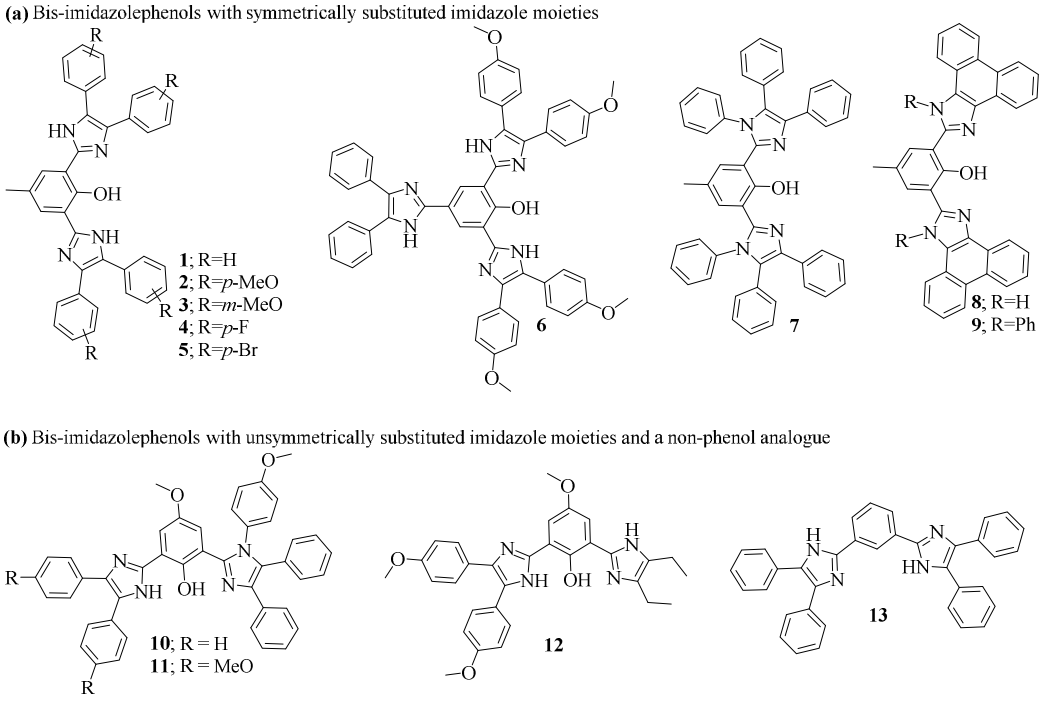

Scheme 2: Structures of fluorophores investigated in this submission; **(a)** Bis-imidazolephenols **1** – **9** with symmetrically substituted imidazole rings, **(b)** Bis-imidazolephenols **10** – **11** with unsymmetrical imidazole substitution and a bis-imidazolephenyl ligand **13** without central hydroxyl function

2. Experimental

2.1 General information

All starting materials for syntheses as well as salts for metal ion sensing experiments were commercially obtained as reagent grades. The compound **1** was prepared according to our previous report.[26] Reactions prone to oxidation were carried out under nitrogen atmosphere using

View Article Online
DOI: 10.1039/C8NJ01265B

standard Schlenk techniques. In order to exclude impurities, the organic compounds were either purified on silica gel columns or re-crystallized. Elemental analyses were performed on Leco CHNS-932 or El Vario III elemental analyzers. ^{1}H and ^{13}CNMR spectra were recorded on Bruker 400 or 600 MHz instrument. IR spectra were recorded on Bruker Equinox spectrometer equipped with a diamond ATR unit.

2.2 Preparation of ligands

2,6-bis(4,5-bis(4-methoxyphenyl)-1H-imidazol-2-yl)-4-methylphenol (**2**): 1,2-bis(4-methoxyphenyl)ethane-1,2-dione (2.00 g, 7.4 mmol), 2-hydroxy-5-methylbenzene-1,3-dialdehyde (0.61 g, 3.7 mmol) and ammonium acetate (16.00 g, 20.7 mmol) were refluxed in glacial acetic acid (15 mL) for 4 hr, cooled, diluted with distilled water (50 mL) and neutralized with concentrated aqueous ammonia. The resulting mixture was extracted twice with 70 mL chloroform. Silica gel powder was added to the combined organic extracts and then evaporated to dryness. The resulting dry mixture was loaded on prepared silica gel column for purification. Chloroform was used as eluent to exclude some impurities before tetrahydrofuran (THF) was used to elute the target product. The collected product was recrystallized from a THF/n-hexane mixture (v/v, 2:5) to obtain **2** as yellow microcrystalline solid (1.70 g, Yield = 69 %). Mp. 334-335 ^{o}C. Selected IR peaks (ATR, cm^{-1}): ν 3380m, 3034m, 2998m, 2949m, 2831m, 1610s, 1583m, 1243vs, 528s. ^{1}H NMR (400 MHz, DMSO-d6): δ 7.93 (s, 2H), 7.48 (d, J = 8.7 Hz, 8H), 6.97 (d, J = 8.2 Hz, 1H), 3.80 (s, 12H, 4 methyl groups of methoxy substituents), 2.40 (s, 3H, methyl group on phenol ring). ^{13}C NMR (50 MH, DMSO-d6): δ 159.0, 152.03, 144.4, 129.5,

View Article Online
DOI: 10.1039/C8NJ01265B

128.0, 127.2, 114.44, 55.6, 20.8. MS (EI) m/z 664 (M^+, 100 %): 664, 649, 332. Anal. Calc. for $C_{41}H_{36}N_4O_5$: C, 74.08; H, 5.46; N, 8.43 %. Found: C, 73.84; H, 5.55; N, 8.44 %.

2,6-bis(4,5-bis(3-methoxyphenyl)-1H-imidazol-2-yl)-4-methylphenol (**3**): 1,2-bis(3-methoxyphenyl)ethane-1,2-dione (0.76 g, 2.8 mmol), 2-hydroxy-5-methylbenzene-1,3-dialdehyde (0.23 g, 1.4 mmol) and ammonium acetate (2.16 g, 28.0 mmol) were reacted and extracted in similar manner as for **2** above, but purification was carried out using a THF/n-hexane solvent mixture (v/v, 1/1) as eluent to obtain **3** as greenish yellow crystalline needles (0.79 g, Yield = 85 %). Mp. 175-176 ^oC. Selected IR peaks (ATR, cm^{-1}): ν 3308m, 2992w, 2913m, 2833m, 1583vs, 1463vs, 1229vs, 697vs. ^1H NMR (600 MHz, DMSO-d6): δ 14.05br (s, 1H), 12.57br (s, 2H, imidazole protons), 7.96 (s, 2H), 7.38br (s, 4H), 7.14 (s, 8H), 6.92 (d, J = 47.6 Hz, 4H), 3.74 (s, 12H, 4 methyl groups of methoxy substituents), 2.41 (s, 3H, methyl group on phenol ring). ^{13}C NMR (101 MHz, DMSO-d6) δ 159.66, 145.8, 134.6, 131.2, 130.0, 120.6, 113.7, 113.3, 55.4 (methoxy), 31.2 (methyl on phenol ring). MS (EI) m/z 664 (M^+, 100 %): 664, 135, 107. Anal. Calc. for $C_{41}H_{36}N_4O_5$: C, 74.08; H, 5.46; N, 8.43 %. Found: C, 74.14; H, 5.81; N, 8.27 %.

2,6-bis(4,5-bis(4-fluorophenyl)-1H-imidazol-2-yl)-4-methylphenol (**4**): 1,2-bis(4-fluorophenyl)ethane-1,2-dione (0.84 g, 3.4mmol), 2-hydroxy-5-methylbenzene-1,3-dialdehyde (0.23 g, 1.4mmol) and ammonium acetate (0.28 g, 1.7mmol) were reacted and extracted in similar manner as for **2** above, but the product was recrystallized from THF/n-hexane mixture (v/v, 2:5) as eluent to obtain **4** as milky solid (0.45 g, Yield = 43 %). Mp. 356-357 ^oC. Selected IR peaks (ATR, cm^{-1}): ν 3398m, 3048w, 1607m, 1593m, 1511s, 1484s, 834vs, 521s. ^1H NMR

View Article Online
DOI: 10.1039/C8NJ01265B

(400 MHz, DMSO-d6) δ 7.85 (s, 2H), 7.55 (dd, J = 8.7, 5.6 Hz, 8H), 7.22 (t, J = 8.9 Hz, 8H), 2.34 (s, 3H, methyl group on phenol ring). ^{13}C NMR (101 MHz, DMSO-d6): δ 173.2 (acetic acid), 160.5, 147.1, 130.0, 130.0, 116.6, 116.0, 115.8, 22.7, 20.8 (acetic acid). MS (EI) m/z 616 (M^+, 100 %): 616, 386, 308, 201. Anal. Calc. for $C_{37}H_{24}F_4N_4O \cdot {}^1/_2THF \cdot {}^1/_2H_2O$: C, 71.01; H, 4.13; N, 8.49 %. Found: C, 71.27; H, 4.49; N, 8.36 %.

2,6-bis(4,5-bis(4-fluorophenyl)-1H-imidazol-2-yl)-4-methylphenol (5): 1,2-bis(4-bromophenyl)ethane-1,2-dione (4.08 g, 11.1mmol), 2-hydroxy-5-methylbenzene-1,3-dialdehyde (0.91 g, 5.5mmol) and ammonium acetate (12.60 g, 0.16 mol) were reacted in acetic acid (20 mL) in similar manner as for **2** above, but the crude, light-green product filtered after dilution with water and neutralization was dried and recrystallized from THF (3.25 g, Yield = 95 %). Mp. 349-350^{o}C. Selected IR peaks (ATR, cm^{-1}): ν 3612w, 3464w, 3391m, 1663m (acetic acid), 1602m, 1480s, 1396m, 827vs, 508s. ^{1}H NMR (400 MHz, DMSO-d6): δ 7.91 (s, 1H), 7.86 (s, 2H), 7.61 (d, *J* = 7.7 Hz, 4H), 7.48 (d, *J* = 7.5 Hz, 4H). ^{13}C NMR (101 MHz, DMSO-d6) δ 133.06, 132.1, 132.1, 130.6, 130.4, 130.3, 130.3, 130.3, 130.2. Anal. calc. for $C_{37}H_{24}Br_4N_4O \cdot 2THF$: C, 53.81; H, 4.01; N, 5.58 %. Found: C, 53.99; H, 3.58; N, 5.97 %.

2,6-bis(4,5-bis(4-methoxyphenyl)-1H-imidazol-2-yl)-4-(4,5-diphenyl-1H-imidazol-2-yl)phenol (**6**): This was obtained in three steps as follows:

(i) Preparation of 4-(4,5-Diphenyl-1H-imidazol-2-yl)phenol intermediate (**I_1**): 4-hydroxybenzaldehyde (3.00 g, 24.6 mmol), benzil (5.10 g, 24.6 mmol) and NH_4OAc (28.00 g, 0.36 mol) were dissolved in 20 mL glacial acetic acid and stirred under reflux for 3 hours.

View Article Online
DOI: 10.1039/C8NJ01265B

Afterwards, the mixture was cooled and water was added until the precipitation is completed. The obtained white solid was extracted with dichloromethane, concentrated by rotary evaporator and the solid precipitate was filtered and dried, which gave the pure product quantitatively as established by NMR.

(ii) Preparation of 5-(4,5-Diphenyl-1H-imidazol-2-yl)-2-hydroxyisophthalaldehyde (**I_2**) and 2-hydroxy-5-(4,5-diphenyl-1H-imidazol-2-yl)benzaldehyde (**I_3**): The intermediate product **I_1** (2.00 g, 6.4 mmol), urotropine (3.6 g, 25.0 mmol), TFA (40 mL) and 0.5 mL TFAA were stirred under reflux for 96 hours. After the reaction, the mixture was cooled down to room temperature and water was added until no further precipitation of solid could be observed. Extraction of the crude product with dichloromethane followed by evaporation of the solvent lead to an orange solid, which was proven to be a mixture that would not be distinctly separable by column chromatography according to TLC checks. Further analysed by NMR and mass spectrometry analyses showed that a mixture of the mono- and di-formylated products (**I_2** + **I_3**) were present in the crude product. Therefore, in hope that solubility difference will become significant for the subsequent imidazole condensation products, the crude formyl product mixture was used directly for the next reaction.

(iii) The crude mixture of **I_2** + **I_3** (from reaction (ii) above), 4,4'-dimethoxybenzil (3.47 g, 7.3 mmol) and NH_4OAc (15.00 g, 194.6 mmol) were combined in 20 mL glacial acetic acid and stirred under reflux for 48 h. Further purification was achieved by column chromatography over silica gel (ethylacetate/n-hexane 1:1) to elute mobile fractions, which yielded 2-(4,methoxyphenyl)-1H-imidazol-2-yl)-4-(4,5-diphenyl-1H-imidazol-2-yl)phenol (0.32 g, Yield = 9 % based on the reactant stoichiometry in reaction (ii) above, see supporting information S1). Subsequently, THF was used to elute the poorly mobile fraction, which was concentrated and the

View Article Online
DOI: 10.1039/C8NJ01265B

precipitate recrystallized by chloroform to obtain the pure products **6** (1.10 g, Yield = 20 % based on the reactant stoichiometry in reaction (ii) above). Mp. 369 ^{o}C. Selected IR peaks (ATR, cm^{-1}): ν 2940w, 2838w, 1654s, 1639s, 1612s, 793vs, 697s. ^{1}H NMR (400 MHz, DMSO-d6): δ 8.75 (s, 2H, phenol ring), 7.58 (d, *J* = 7.3 Hz, 4H), 7.50 (d, *J* = 8.8 Hz, 8H), 7.43 (t, *J* = 7.4 Hz, 4H), 7.37 (d, *J* = 7.2 Hz, 2H), 7.04 (d, *J* = 8.8 Hz, 8H), 3.81 (s, 12H, methoxy). ^{13}C NMR (101 MHz, DMSO-d6): δ 172.5, 159.9, 158.4, 150.8, 145.1, 144.7, 142.7, 130.0, 129.0, 128.3, 127.8, 122.5, 114.8, 114.5, 55.7, 21.5. Anal. Calc. for $C_{55}H_{44}N_6O_5 \cdot 2H_2O \cdot CHCl_3$: C, 65.66; H, 4.82; N, 8.20 %. Found: C 65.69, H 4.48, N 7.71 %.

4-methyl-2,6-bis(1,4,5-triphenyl-1H-imidazol-2-yl)phenol (**7**): Benzil (3.07 g, 14.6 mmol), 4,6-dihydroxy-5-methylbenzene-1,3-dialdehyde (1.20 g, 7.3 mmol), aniline (1.91 g, 20.5 mmol, 1.4 equivalent) and ammonium acetate (3.38 g, 43.9 mmol, 3 equivalent) were reacted and extracted in similar manner as for **2** above, but purification was on silica gel column using a chloroform/n-hexane mixture (1:5) as eluent to obtain **7** as milky solid (4.4 g, Yield = 87 %), which was recrystallized in THF. Mp. 297 ^{o}C. Selected IR peaks (ATR, cm^{-1}): ν 3049m, 2914m, 1597m, 1495s, 1467s, 694vs, 655s. ^{1}H NMR (400 MHz, $CDCl_3$): δ 13.47 (s, 1H, hydroxyl proton), 7.52 (d, J = 7.3 Hz, 4H), 7.30-7.15 (m, 26H), 6.68 (s, 2H), 1.81 (s, 3H, methyl group on phenol ring). ^{13}C NMR (101 MHz, $CDCl_3$): δ 155.0, 145.2, 137.2, 131.2, 130.5, 130.0, 128.9, 128.4, 128.3, 128.06, 127.3, 126.6, 126.1, 20.4 (methyl on phenol ring). MS (EI) m/z 696 (M^+, 100 %): 620, 696, 348. Anal. calc. for $C_{49}H_{36}N_4O \cdot ½$ THF: C, 83.58; H, 5.50; N, 7.64 %. Found: C 83.88, H 5.78, N 7.52 %.

View Article Online
DOI: 10.1039/C8NJ01265B

4-methyl-2,6-di(1H-phenanthro[9,10-d]imidazol-2-yl)phenol (**8**): Phenanthrene-9,10-dione (2.00 g, 9.6 mmol), 2-hydroxy-5-methylbenzene-1,3-dialdehyde (0.79 g, 4.8 mmol) and ammonium acetate (11.11 g, 144.1 mmol) were treated as for **2** above. The poorly soluble crude product was filtered off after neutralization to obtain **8** as yellow amorphous solid, which was found to be spectroscopically pure (2.58 g, Yield = 99 %). Mp. 191 ^{o}C. Selected IR peaks (ATR, cm^{-1}): ν 3050m, 1650m, 1631m, 1542s, 744vs, 672vs, 614s. ^{1}H NMR (400 MHz, DMSO-d6): δ 13.80 (s, 2H, imidazole proton), 8.90 (d, *J* = 8.3 Hz, 4H), 8.68 (d, *J* = 7.9 Hz, 4H), 8.23 (s, 2H), 7.79 (t, *J* = 7.5 Hz, 4H), 7.69 (t, *J* = 7.4 Hz, 4H), 2.54 (s, 3H, methyl group on phenol ring), peaks corresponding to acetic acid observed (see supporting information). ^{13}C NMR (101 MHz, DMSO-d6) δ 172.47, 153.5, 148.5, 128.6, 128.3, 127.7, 126.1, 124.5, 122.6, 122.5, 21.5, 20.9. MS (EI) m/z 540 (M^{+}, 100 %): 540, 380, 348, 319. Anal. calc. for $C_{37}H_{24}N_4O$: C, 82.20; H, 4.47; N, 10.36 %. Found: C, 81.9; H, 4.50; N, 10.05 %.

4-methyl-2,6-bis(1-phenyl-1H-phenanthro[9,10-d]imidazol-2-yl)phenol (**9**): Phenanthrene-9,10-dione (2.00 g, 9.6 mmol), 2-hydroxy-5-methylbenzene-1,3-dialdehyde (0.79 g, 4.8 mmol), aniline (0.89 g, 9.6 mmol) and ammonium acetate (2.22 g, 28.8 mmol, 3 equivalent) were reacted and extracted as in the preparation of **2** above. Silica gel was added to the extract and the slurry dried by evaporation. Purification was carried out on silica gel column firstly by a chloroform/n-hexane mixture (2/3) and later with higher chloroform ratio to obtain **9** as yellow powder that was then crystallized from THF (0.11 g isolated yield, Yield = 3 %). Mp. >400 ^{o}C. Selected IR peaks (ATR, cm^{-1}): ν 3056m, 2913w, 1677m, 1609m, 1596m, 1450s, 750vs, 721vs, 694vs. ^{1}H NMR (400 MHz, DMSO-d6): δ 8.95 (d, *J* = 8.3 Hz, 4H), 8.90 (d, *J* = 8.2 Hz, 2H), 8.59 (d, *J* = 7.8 Hz, 2H), 7.84 – 7.67 (m, 14H), 7.58 (t, *J* = 7.7 Hz, 4H), 7.36 (t, *J* =

View Article Online
DOI: 10.1039/C8NJ01265B

7.6 Hz, 2H), 7.08 (d, J = 8.2 Hz, 2H), 6.93 (s, 2H), 1.89 (s, 3H). ^{13}C NMR (101 MHz, DMSO-d6): δ 159.6, 155.8, 149.1, 149.0, 138.7, 138.4, 131.9, 130.8, 130.1, 129.2, 129.0, 127.5, 125.6, 122.3, 120.8, 117.1, 116.9, 20.4. MS (EI) m/z 692 (M^+, 100 %): 692, 348, 267. Anal. calc. for $C_{49}H_{32}N_4O$·½ THF: C, 83.81; H, 5.24; N, 7.67 %. Found: C 84.48, H 5.10, N 7.62 %.

4-methoxy-2-(1-(4-methoxyphenyl)-4,5-diphenyl-1H-imidazol-2-yl)-6-(4,5-diphenyl-1H-imidazol-2-yl)phenol (**10**): Two reaction steps were involved. (i) Preparation of 2-Hydroxy-5-methoxy-3-(3-(4-methoxyphenyl)-4,5-diphenyl-1H-3l4-imidazol-2-yl)benzaldehyde (**I_4**) via *ortho*-formylation reaction of substituted phenols - 4-Methoxy-2-(3-(4-methoxyphenyl)-4,5-diphenyl-1H-imidazol-2-yl)phenol (3.00 g, 6.7 mmol) prepared from one of our ongoing projects and an excess of urotropine (1.8 g, 13.0 mmol) were dissolved in trifluoroacetic acid (tfa, 30 mL) and trifluoroacetic acid anhydride (tfaa, 0.5 mL). The mixture was stirred under reflux for overnight. After the reaction mixture was cooled to room temperature, water was added until no further precipitation of solid could be observed. The resulting reaction mixture was extracted with chloroform followed by purification by silica column chromatography (n-hexane/ethanol, initially 3:4, later 1:1). The pure intermediate product (**I_4**) was obtained as a white solid (2.77 g, Yield = 87 %) confirmed by mass spectrometry.

(ii) 4-methoxy-2-(1-(4-methoxyphenyl)-4,5-diphenyl-1H-imidazol-2-yl)-6-(4,5-diphenyl-1H-imidazol-2-yl)phenol (**10**): The precursor **I_4** (1.37g, 2.9mmol.), benzil (0.60 g, 2.9mmol) and ammonium acetate (3.32 g, 43.1mmol.) were reacted as in the preparation of **2** above. The precipitate obtained after neutralization and filtration was purified on silica gel by first applying chloroform, which excluded benzil and some other small impurities. A repeat column was then

View Article Online
DOI: 10.1039/C8NJ01265B

made with 2 n-hexane: 1 ethyl acetate to obtain **10** as yellow crystalline solid (1.02 g, Yield = 53 %). Mp. = 289 ^{o}C. Selected IR peaks (ATR, cm^{-1}): ν 3601m, 3398m, 3378s, 3054m, 3001m, 2951vs, 2924vs, 2854s, 1731s, 1602s, 1579s, 1508s, 578vs. ^{1}H NMR (400 MHz, $CDCl_3$): δ 11.37 (s, 1H), 8.03 (d, *J* = 3.0 Hz, 4H), 7.67 (s, 10H), 7.58 (d, *J* = 7.0 Hz, 8H), 7.39 (s, 15H), 7.34 – 7.25 (m, 41H), 7.21 – 7.16 (m, 18H), 6.93 (d, *J* = 8.9 Hz, 9H), 6.32 (d, *J* = 3.1 Hz, 4H), 3.84 (s, 14H), 3.55 (s, 14H). ^{13}C NMR (101 MHz, $CDCl_3$) δ 160.1, 151.5, 149.7, 144.8, 144.5, 135.0, 133.0, 131.4, 131.1, 129.8, 129.6, 128.5, 128.3, 127.9, 127.2, 127.0, 114.9, 113.8, 112.4, 55.6, 55.5. Anal. calc. for $C_{44}H_{34}N_4O_3 \cdot ½H_2O$: C, 78.20; H, 5.22; N, 8.29 %. Found C 78.56, H 5.17, N 8.24 %.

2-(4,5-bis(4-methoxyphenyl)-1H-imidazol-2-yl)-4-methoxy-6-(1-(4-methoxyphenyl)-4,5-diphenyl-1H-imidazol-2-yl)phenol (**11**): The precursor **I_4** (1.40 g, 2.9 mmol.), 1,2-bis(4-methoxyphenyl)ethane-1,2-dione (1.01 g, 3.7 mmol) and ammonium acetate (3.40 g, 44.1 mmol) were reacted as in the preparation of **2** above in addition to nitrogen protection. The crude product was purified on silica gel using chloroform–ethyl acetate (100:15) as eluent to obtain **11** as yellow crystalline solid (1.64 g, Yield = 77 %). Mp. = 181-182 ^{o}C. Selected IR peaks (ATR, cm^{-1}): ν 3391m, 3036w, 2995w, 2933w, 2833m, 1609s, 1580m, 1510vs, 1244vs, 536s. ^{1}H NMR (400 MHz, $CDCl_3$): δ 8.05 (s, 1H), 7.57 (d, *J* = 7.3 Hz, 6H), 7.35 – 7.24 (m, 17H), 7.21 – 7.16 (m, 6H), 6.93 (d, *J* = 8.6 Hz, 8H), 6.31 (d, *J* = 2.6 Hz, 1H), 3.86 (s, 8H), 3.85 (s, 6H), 3.56 (s, 4H). ^{13}C NMR (101 MHz, $CDCl_3$) δ 135.0, 131.4, 131.0, 130.6, 129.9, 129.7, 129.1, 128.5, 128.4, 128.3, 127.8, 127.0, 122.8, 114.93, 55.7, 55.3. Anal. calc. for $C_{46}H_{38}N_4O_5 \cdot$ THF: C, 75.17; H, 5.80; N, 7.01 %. Found C, 75.11; H, 5.95; N, 7.04 %.

View Article Online
DOI: 10.1039/C8NJ01265B

2-(4,5-bis(4-methoxyphenyl)-1H-imidazol-2-yl)-6-(4,5-diethyl-1H-imidazol-2-yl)-4-methoxyphenol (**12**): This product was obtained by three steps in which the first step was conducted in two reaction media; (i_a) ethanol under nitrogen protection with catalytic amount of acetic acid or (i_b) acetic acid without nitrogen protection.

(i_a) Preparation of 2-(4,5-Diethyl-1H-imidazol-2-yl)-4-methoxyphenol (**I_5**): In a Schlenk tube NH_4OAc (32.00 g, 0.42 mol) was dissolved in 40 mL dry and degassed ethanol under inert conditions. While stirring 2-Hydroxy-5-methoxybenzaldehyde (3.5 mL, 28.0 mmol), 3,4-hexanedione (3.5 mL, 28.8 mmol) and 0.5 mL glacial acetic acid were added via syringe. After refluxing for overnight, the crude reaction mixture was treated as for ligand **2** to obtain **I_5** (0.48 g, Yield = 7 %). MS (EI) m/z 246 (M^+, 100 %): 246, 231, 203, 159.

(i_b) Owing to the low yield in the above reaction in ethanol, use of excess 3,4-hexanedione was considered for trial. Ammonium acetate (22.04 g, 0.42 mol), 2-hydroxy-5-methoxybenzaldehyde (2.90 g, 19.1mmol), 3,4-hexanedione (10.90 g, 95.3mmol) and 5 mL glacial acetic acid were refluxed without inert atmosphere overnight, cooled, diluted with 150 mL distilled water and extracted trice with 50 mL dichloromethane. The combined extracts were concentrated and crystals of **I_5** that grew on standing were filtered (3.68 g, Yield = 78 %).

(ii) 3-(4,5-Diethyl-1H-imidazol-2-yl)-2-hydroxy-5-methoxybenzaldehyde (**I_6**): The product **I_5** (2.30 g, 9.4 mmol), urotropine (1.96 g, 1.4 mmol) and TFA (25 mL) were stirred under reflux for 48 h. After the reaction the mixture is cooled down to room temperature, water is added until no further precipitation of solid can be observed and subsequently extracted trice with chloroform. The combined extract was evaporated under vacuum, which gave dark oil.

View Article Online
DOI: 10.1039/C8NJ01265B

Filtration over silica with THF gave **I_6** as dark oil, which was used directly in the next reaction. The product was confirmed via mass spectrometry. MS (EI) m/z 274 (M^+, 100 %): 274, 245, 231, 203.

(iii) Preparation of ligand **12**: The product **I_6** (as obtained from reaction (ii) above), 4,4'-dimethoxybenzil (2.53 g, 9.36 mmol) and NH_4OAc (12.00 g, 0.16 mmol) were reacted according to procedure for **2** for 20 h. After the addition of water, the mixture was extracted directly with dichloromethane followed by concentration under reduced pressure. Further purification was carried out by column chromatography over silica gel (n-hexane/ethylacetate, initially 7:5, later 5:7) to obtain **12** as yellow powder (0.95 g, Yield = 19 %). Suitable crystal was grown by slow evaporation of chloroform solution of **12**. Mp. 336-337 ^oC. Selected IR peaks (ATR, cm^{-1}): ν 3390s, 3068m, 2964s, 2931s, 2836, 1614s, 1595s, 1572s, 1530s, 1485vs, 823vs, 522s. ^1H NMR (400 MHz, $CDCl_3$): δ 7.67 (s, 1H), 7.49 (d, J = 8.0 Hz, 4H), 7.29 (s, 1H), 6.88 (d, J = 8.5 Hz, 4H), 3.83 (s, 6H), 3.75 (s, 3H), 2.63 (d, J = 6.1 Hz, 4H), 1.26 (t, J = 7.6 Hz, 6H). ^{13}C NMR (101 MHz, CDCl3): δ 159.0, 143.1, 129.1, 126.8, 114.1, 58.3, 55.24, 18.7, 14.3. MS (EI) m/z 524 (M^+, 100 %): 524, 509 (loss of 1 methyl), 481 (loss of 3 methyl groups). Anal. calc. for $C_{31}H_{32}N_4O_4$: C, 70.97; H, 6.15; N, 10.68 %. Found: C, 72.32; H, 6.44; N, 10.70 %.

4,5-diphenyl-2-(3-(4,5-diphenyl-1H-imidazol-2-yl)phenyl)-1H-imidazole (**13**): Isophthalaldehyde (0.51 g, 3.8 mmol), benzil (1.59 g, 7.6 mmol) and ammonium acetate (5.84 g, 75.8mmol) were reacted as for **2**. The reaction mixture was cooled and the resulting precipitates were filtered, washed with acetic acid (ca. 30ml) and n-hexane (ca. 20ml). Column chromatography was then performed using an ethyl acetate/n-hexane mixture (1/4) followed by

View Article Online
DOI: 10.1039/C8NJ01265B

recrystallization from n-hexane/ethyl acetate mixture to obtain **13** as white solid (0.39 g, 20 %). Mp. 212 ^{o}C. Selected IR peaks (ATR, cm^{-1}): ν 3629m, 3290m, 3049m, 1714s, 1582s, 1481s, 763vs, 694vs.^{1}H NMR (600 MHz, DMSO-d6): δ 12.86 (s, 1H), 8.82 (s, 1H), 8.09 (dd, *J* = 7.8, 1.6 Hz, 1H), 7.63 – 7.58 (m, 3H), 7.54 (d, *J* = 7.2 Hz, 2H), 7.46 (t, *J* = 7.6 Hz, 2H), 7.39 (t, *J* = 7.4 Hz, 1H), 7.33 (t, *J* = 7.6 Hz, 2H), 7.25 (t, *J* = 7.3 Hz, 1H), 2.00 (s, 1H, acetic acid).^{13}C NMR (151 MHz, DMSO-d6): δ 145.8, 137.8, 135.6, 131.5, 131.4, 129.1, 129.0, 128.9, 128.7, 128.3, 127.7, 127.1, 125.4, 122.8, 60.2, 21.2. MS (EI) m/z 514 (M^{+}, 100 %): 514, 411, 324, 257, 165. Anal. calc. for $C_{36}H_{26}N_4 \cdot 2H_2O \cdot HAcO$: C, 77.01; H, 5.44; N, 9.45 %. Found: C 77.10, H 4.99, N 9.63 %.

2.3 Structure determinations

The intensity data for the compounds were collected on a Nonius Kappa CCD diffractometer using graphite-monochromated Mo-K_α radiation. Data were corrected for Lorentz and polarization effects; absorption was taken into account on a semi-empirical basis using multiple-scans.[31] The structures were solved by direct methods (SHELXS)[32] and refined by full-matrix least squares techniques against F_o^2 (SHELXL-97).[32] The hydrogen atoms of the X-ray data of compounds **12** and **7**-$CoCl_2$ were located by difference Fourier synthesis and refined isotropically. All other hydrogen atoms were included at calculated positions with fixed thermal parameters. All non-disordered heavy atoms were refined anisotropically. The crystallographic data as well as structure solution and refinement parameters for **12** and **7**-$CoCl_2$ are collected in Table 1. Structural data for the self-assembled compounds **1**-$Co(OAc)_2$, **2**-$Cd(ClO_4)_2$, **2**-H_2ClO_4 and **2**-$Zn(ClO_4)_2$ were obtained with *R* values in the range of 10-17 %, due to the low quality of the crystals. Nonetheless, the data sets are sufficient to show connectivity and geometry for the

View Article Online
DOI: 10.1039/C8NJ01265B

respective species (see supplementary information Table S1 for their crystallographic data as well as structure solution and refinement details). XP (SIEMENS Analytical X-ray Instruments, Inc.) was used for structure representations.[33]

Table 1: Crystal data and refinement details for the X-ray structure determinations of the compounds **12** and **7**-$CoCl_2$**.**

Compound	**12**	**7**-$CoCl_2$
formula	$C_{31}H_{32}N_4O_4$	$C_{49}H_{36}Cl_2CoN_4O$
fw ($g \cdot mol^{-1}$)	524.61	826.65
T(°C)	-140(2)	-140(2)
crystal system	monoclinic	triclinic
space group	P 2_1/n	P $\bar{1}$
a/ Å	11.7841(2)	10.9294(4)
b/ Å	11.7123(2)	11.1711(3)
c/ Å	20.2881(4)	17.8224(4)
α/°	90	75.494(2)
β/°	104.441(1)	83.788(2)
γ/°	90	71.540(1)
V/Å^3	2711.67(8)	1997.2(1)
Z	4	2
ρ ($g \cdot cm^{-3}$)	1.285	1.375
μ (cm^{-1})	0.86	6.07

View Article Online
DOI: 10.1039/C8NJ01265B

measured data	16866	15767
data with I > 2σ(I)	5127	7181
unique data (R_{int})	6190/0.0322	8649/0.0317
wR_2 (all data, on F^2)[a]	0.1203	0.1063
R_1 (I> 2σ(I))[a]	0.0475	0.0492
S[b]	1.069	1.092
Res. dens./e·Å^{-3}	0.286/-0.215	0.513/-0.437
Absorpt method	multi-scan	multi-scan
Absorpt corr $T_{min/max}$	0.6477/0.7456	0.6901/0.7456
CCDC No.	1505094	1505093

[a]Definition of the R indices: $R_1 = (\Sigma || F_o | - | F_c ||)/\Sigma | F_o |$; $wR_2 = \{\Sigma[w(F_o^2-F_c^2)^2]/\Sigma[w(F_o^2)^2]\}^{1/2}$ with $w^{-1} = \sigma^2(F_o^2) + (aP)^2+bP$; $P = [2F_c^2 + Max(F_O^2]/3$; [b]$s = \{\Sigma[w(F_o^2-F_c^2)^2]/(N_o-N_p)\}^{1/2}$.

2.4 Measurements of spectroscopic sensing properties

Typically, a 10^{-5} M solution of a ligand in a solvent was prepared in 100 mL standard flask. 10^{-3} M solutions of various metal ions were also prepared in 50 mL standard flasks and the nitrate salts were generally sought after for solubility reasons. Eppendorf pipette was used to deliver 3 mL of the ligand solutions into a 1 cm × 1 cm quartz cuvette equipped with a tiny magnetic bar. After acquiring the UV absorption as well as the fluorescence excitation and emission spectra of the free ligand in solution, the needed amount (typically 3 equivalents except in the case of titrations) of a given metal ion was then added by Eppendorf micro-pipetteor micro-syringe and the mixture stirred for ~10 seconds before repeat measurement of the UV and fluorescence data for the response emission signals in the presence of the added cations. Similar

View Article Online
DOI: 10.1039/C8NJ01265B

procedure was repeated in other solvents, with other equivalents of the metal ion or in the presence of varying acid anions and base condition.

2.5 Quantum yields

Quantum yields were obtained by the relative method as defined by equation (1). The fluorescent quantum yields $\Phi_{F,x}$ and $\Phi_{F,std}$, the fluorescent intensities as a function of wavelength $I_{F,x}(\nu)$ and $I_{F,std}(\nu)$, the absorbance values A_x and A_{std} and the refractive indices for the corresponding solvent media n_x and n_{std} denote the values for the sample *x* and the standard, respectively. Anthracene in ethanol ($\Phi_{F,std} = 0.27$) was used as standard.[34]

$$\Phi_{F,x} = \Phi_{F,std} \frac{\int I_{F,x}(\nu) d\nu}{\int I_{F,std}(\nu) d\nu} \left(\frac{1-10^{-A_{std}}}{1-10^{-A_x}} \right) \left(\frac{n_x}{n_{std}} \right)^2 \quad (1)$$

2.6 Job plot

In the Job plot experiment aimed at estimating molecular stoichiometry of the metal-ligand species responsible for fluorescent response in sensor action, stock solutions of the ligand and metal ions were prepared at 10^{-5} M concentrations. The experiment was performed using 3mL solutions made up of combination the appropriate volumes of the stock solutions of the sensor candidate and metal ion (i.e. mL volume ratios of 3:0, 2.7:0.3, 2.4:0.6, 2.1:0.9, 1.8:1.2, 1.5:1.5, 1.2:1.8, 0.9:2.1, 0.6:2.4, 0.3:2.7 and 0:3 providing metal ion mole fractions of 0.0, 0.1, 0.2, 0.3, 0.4, 0.5, 0.6, 0.7, 0.8, 0.9 and 1.0, respectively). Spectral data were measured for the solutions and the plot of spectral peak values against the mole fraction was obtained.[35]

View Article Online
DOI: 10.1039/C8NJ01265B

2.7 Quantum mechanical calculations

Geometries of model structures (*see below*) are optimised with def2-SV(P) basis and B3LYP functional using TURBOMOLE suite of programs.[36] Energies of electronic ground state and excited states are obtained as roots of diagonalised configuration interaction (CI) hamiltonian in many-electron basis of spin and symmetry restricted Slater determinants. These Slater determinants are built of one-electron orbitals optimized in multiconfigurational self consistent field (MCSCF) over complete active spaces (CAS) or occupation restricted multiple active spaces (ORMAS) of these orbitals. Both state specific and state averaged orbitals were optimized, but results reported here are based on later. State specific orbitals were used to assess the number of electronic states to be included in state averaging. Dynamic correlation is included through second-order multireference perturbation theory (MRPT2)[2, 3, 4, 5].[37,38] The basis set used for these calculations are 6-31+G* and the GAMESS suite of programmes[38] is employed to perform all multiferfernce/multiconfiguration calculations. Time dependent density functional theoretical (TD-DFT) vertical excitation energies for model structures 2L and 2LR (*see below*) are also calculated with def2-TZVP basis and B3LYP functional by using TURBOMOLE program.[36] Results of these calculations are referred to as TD-B3LYP below.

3. Results and discussion

3.1 Syntheses and characterization of the azole compounds

View Article Online
DOI: 10.1039/C8NJ01265B

The designs of the studied compounds **1** - **13** as presented in Scheme 2 were chosen to mildly or significantly modify properties of 2,6-bis(4,5-diphenyl-1H-imidazol-2-yl)-4-methylphenol (i.e. ligand **1**) with reference to electronic, geometry, symmetry and intramolecular interaction settings. All molecular candidates were fully characterized and their synthetic analytical data are consistent with expected values. Some x-ray crystal results also confirmed identities of the studied materials.

Imidazole rings of the compounds **1** – **13** (Scheme 2) were created by condensation of arylaldehyde function, a given α-diketone and excess ammonium acetate in refluxing acetic acid. However, while the formation of the symmetric bis-imidazole ligand compounds **1** – **9** and **13** proceeds easily over a single-step reaction, preparation of the bis-imidazolephenols bearing unsymmetrically substituted imidazole rings (i.e. **10** – **12**) required multi-step procedures via aldehyde intermediate precursors. Unfortunately, it was not possible to achieve stepwise imidazole ring condensation on only one aldehyde functions of the 2-hydroxy-5-methylbenzene-1,3-dialdehyde as each attempt produced the symmetrical analogues illustrated by the reaction equation in Scheme 3 (a). Several attempts to form an imidazole ring at only one aldehyde function largely yielded only the symmetrical bis-imidazole products even when as low as a quarter equivalent of α-diketone reagent was used in dropwise manner. Consequently, compounds **6**, **10** – **12** were obtained by firstly preparing 2-(1H-imidazol-2-yl)phenol precursors from monoaldehydes followed by formylation at *ortho*-position to the hydroxyl group (i.e. Scheme 3 (b)). Subsequently, a different imidazole moiety is then condensed on the newly formed aldehyde function; i.e. Scheme 3 (b), compound **6** obtained from intermediate $\mathbf{I_3}$, compound **10** and **11** from $\mathbf{I_4}$, and compound **12** from $\mathbf{I_6}$.

View Article Online
DOI: 10.1039/C8NJ01265B

The use of aliphatic α-dicarbonyls such as butane-2,3-dione, hexane-3,4-dione, etc. in imidazole syntheses is scarcely reported in literature, which is presumably due to the very low and unattractive yields achievable under the regular stoichiometry of reactants.[39] In our previous use of aliphatic α-dicarbonyls,[27,29,30] low yields were also recorded, which lead to speculations that acetic acid media was too harsh for the aliphatic α-dicarbonyls and that inert atmosphere protection was necessary. It is however interesting to report that this problem can be overcome by utilizing an excess of the α-diketone (5 equivalents). In the current synthesis of 2-(4,5-diethyl-1H-imidazol-2-yl)-4-methoxyphenol (**I_5**), 78 % yield was achieved by applying 5-fold excess of hexane-3,4-dione without nitrogen protection and in refluxing glacial acetic acid. The same reaction with 1.2 equivalent of hexane-3,4-dione conducted in ethanol with catalytic 0.5 mL acetic acid under nitrogen protection yielded only 7 % of the target product.

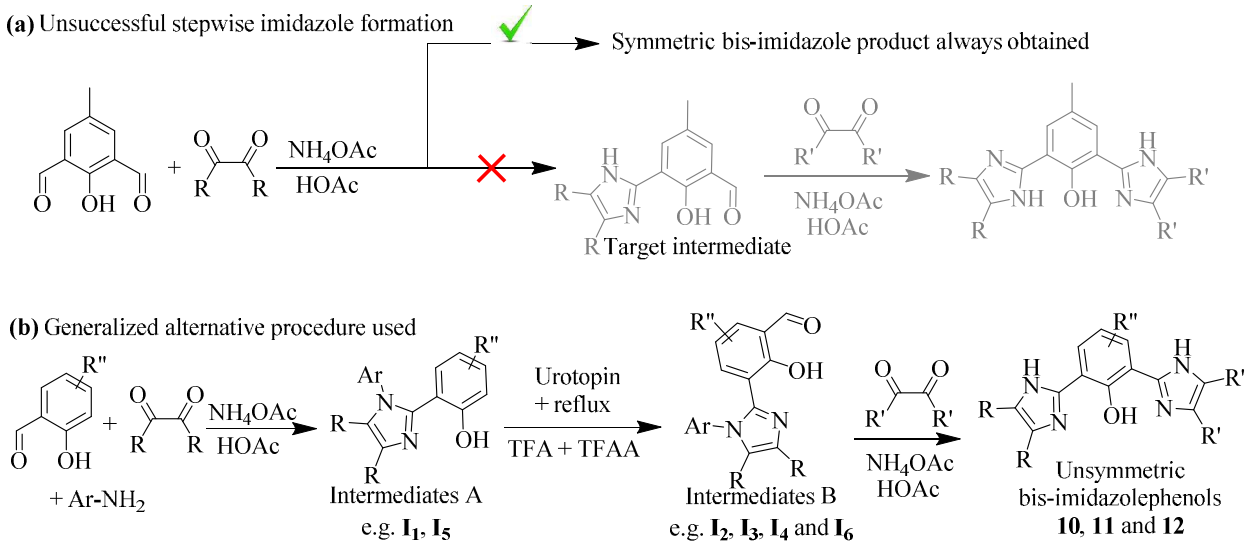

Scheme 3: (a) The unsuccessful mono-imidazole formation from 2-hydroxy-5-methylbenzene-1,3-dialdehyde and (b) the alternative route used to obtain the unsymmetrical bis-

View Article Online
DOI: 10.1039/C8NJ01265B

imidazolephenols **10** – **12** through formylation intermediates (TFA = trifluoroacetic acid and TFAA = trifluoroaceticanhydride)

3.2 Structural analyses

Structural analyses were pursued in order to obtain possible clue about ligand geometrical properties, intramolecular interaction features and available coordination options. Suitable single crystal of ligand **12** (Fig. 1) is obtainable by slow evaporation of solvent from its chloroform solution while crystals for various coordination species were self-assemble by allowing a given metal salt and a given ligand to stand overnight in solvent. Suitable crystals of **7**-$CoCl_2$ (Fig. 2) were self-assembled by standing ligand **7** and cobalt(II) chloride in ethanol.

Structural motifs of **1**-$Co(OAc)_2$, **2**-$Cd(ClO_4)_2$, **2**-$HClO_4$, and **2**-$Zn(ClO_4)_2$) were similarly obtained from corresponding salts and ligands. Their respective *R*-factor values of 10 %, 13 %, 18 % and 12 % are attributed to disordered solvent molecules in large voids. Their perspective views are presented in Fig. 3 for illustrating connectivities in various coordination interactions while their structural parameters are presented in Table S1 of the Supporting Information.

X-ray crystal results for ligands **12** (Fig. 1) and **2** (Fig. 3 (c)) revealed that the studied 2,6-di(1H-imidazol-2-yl)phenol derivatives could possess a relay of two intramolecular hydrogen bonds. This hydrogen bonding relay spans from the N–H proton of one imidazole group over the central phenol OH group to the nitrogen base of the second imidazole ring. For instance, the relay N(1)–H···O(1)–H···N(4) in ligand **12** has hydrogen bond lengths 2.03 Å and 1.71 Å respectively. Presence of at least one unsubstituted imidazole proton as in ligands **1** – **6**, **8** and **10**

View Article Online
DOI: 10.1039/C8NJ01265B

– **12** would be enough for the relay to exist. The same hydrogen bonding relay has also been previously observed by us for compound **1**.[26]

While binuclear N^O^N complexation could be formed as seen in Fig. 3 (a), (b) and (d)), it is interesting that mononuclear 1:1, single-pocket N^O coordination product was also encountered for **7**-$CoCl_2$ (Fig. 2) despite crystallization from saturated solution. Furthermore, it is noteworthy that, despite phenyl-substitution of both imidazole protons of ligand **7** and after deprotonation of the phenolic OH as observed in **7**-$CoCl_2$, there is yet the tendency to stabilize the non-coordinated N^O pocket by intramolecular hydrogen bonding (O1···N3, 2.47 Å). It may be reasonable to suggest that this mononuclear N^O coordination, which yet preserves ESIPT capability, could be the realistic coordinative interaction in such dilute working concentrations as employed during fluorescence sensing experiments (typically 10^{-5} M). While the binuclear N^O^N coordination mode should necessarily obliterate intramolecular hydrogen bonding capabilities, eliminate ESIPT character and cause reduction of the Stoke's shifts, the mononuclear N^O coordination should yet retain these free-ligand features as later established by from spectroscopic results.

View Article Online
DOI: 10.1039/C8NJ01265B

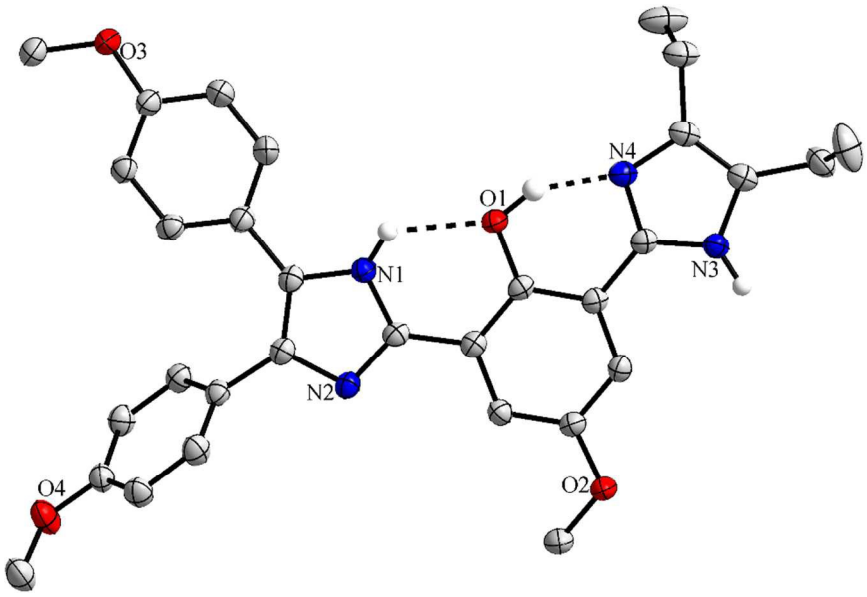

Fig. 1**:** Molecular structure of compound **12** with thermal ellipsoids drawn at the 50 % probability level. Some atomic labels and protons have been omitted for clarity.

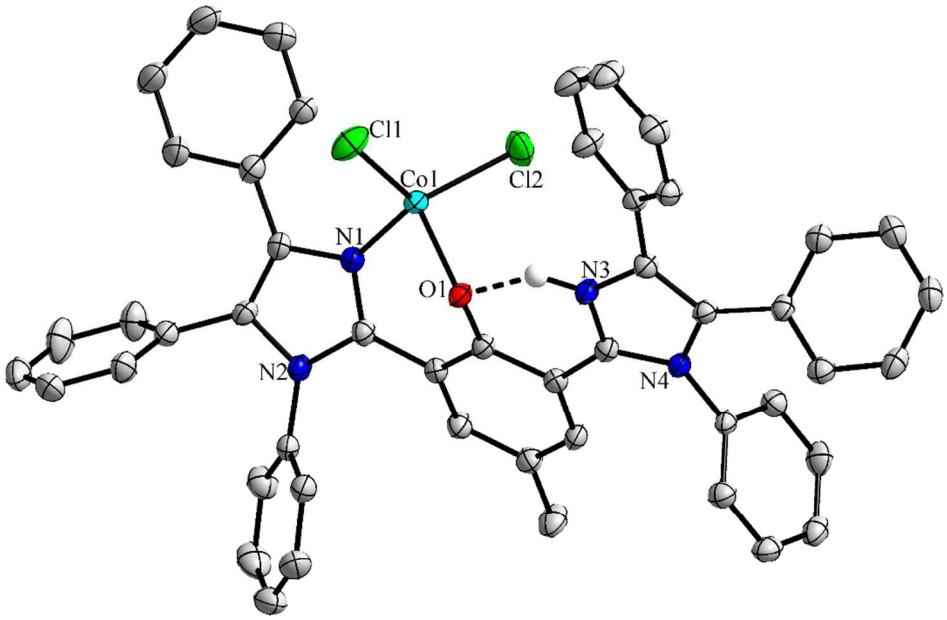

View Article Online
DOI: 10.1039/C8NJ01265B

503 Fig. 2**:** Molecular structure of **7**-$CoCl_2$ with thermal ellipsoids drawn at the 50% probability

504 level. Some atomic labels and protons have been omitted for clarity.

505

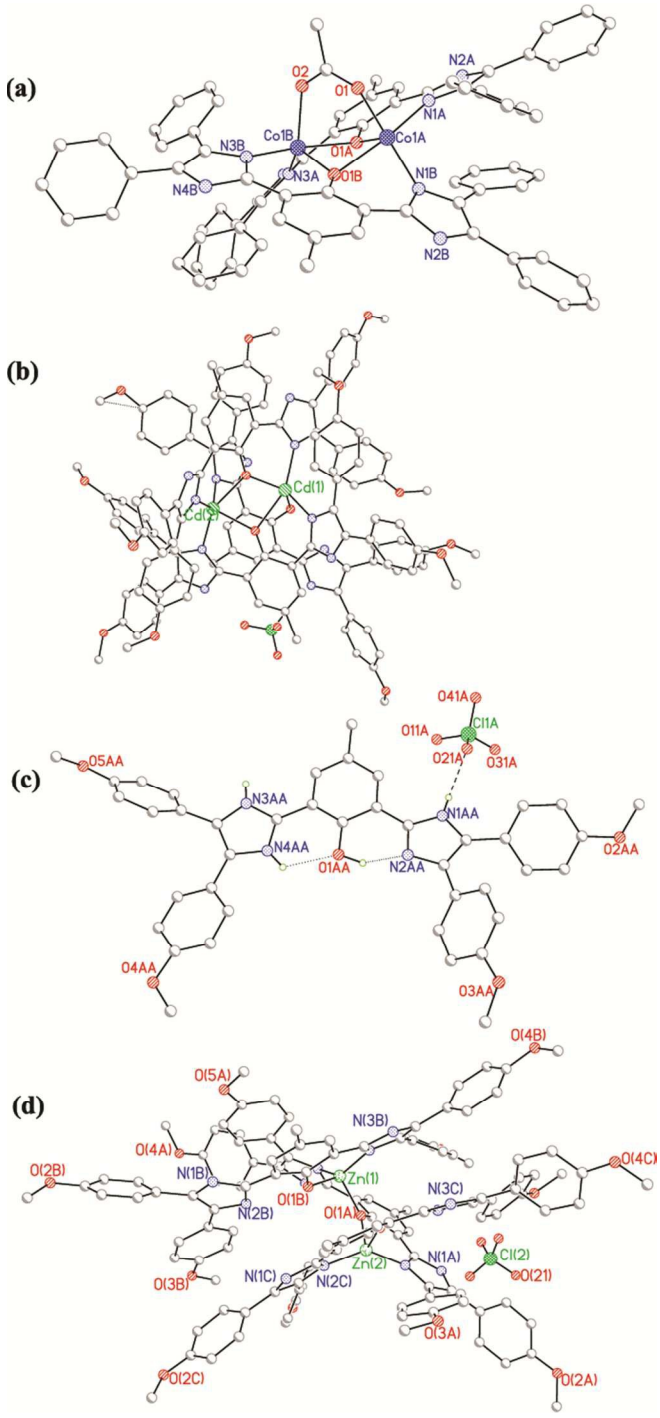

506

View Article Online
DOI: 10.1039/C8NJ01265B

Fig. 3**:** Ball and stick representations of the structural motifs obtained for self-assembled coordination species: (a) **1**-$Co(OAc)_2$, (b) **2**-$Cd(ClO_4)_2$, (c) **2**-$HClO_4$, (d) ligand **2**-$Zn(ClO_4)_2$. Some atomic labels, protons or anions have been omitted for clarity.

3.3 Spectroscopic properties of the ligands

Initially, emission of compound **1** was measured in methanol, ethanol, 1:1 tetrahydrofuran/water mixture, dimethyformamide and acetonitrile. The lowest emission intensity observed in acetonitrile informed conduction of further experiments in acetonitrile (see Fig. S1, supporting information). Data for UV absorption and fluorescent emission of the studied ligands in acetonitrile are collected in Table 2. A notable observation is that the bis-imidazole compounds **1** – **5** in acetonitrile show isoelectronic characteristics based on spectral profiles and peak positions (Fig. 4 (a)). Their longest wavelength absorption bands ($\lambda_{max(abs)}$) are peaked within 349 nm – 356 nm while their next absorption bands also occur within 291 nm – 296 nm. On the other hand, the electronic spectra for ligands **6** – **13** show wide variations in terms of peak positions and spectral profiles (Fig. 4 (a) and (b)).

For ligands **1** – **5**, the UV spectral results reveal the possibility to synthetically manipulate and derivatize the nucleus (i.e. ligand **1**) at the 4,5-diphenyl-rings without severe consequence on its electronic state. Consequently, such substitution centers may be utilized for improving molecular properties or even for grafting the molecule onto a support while yet retaining its robust electronic character. The substituents in ligands **1** – **5** correlated with peak positions as follows: *p*-methoxy for ligand **2** at 356 nm > unsubstituted ligand **1** and *m*-methoxy of ligand **3** at 351 nm > *p*-bromo of ligand **4** and *p*-fluoro of ligand **5** at 349 nm. Although the

View Article Online
DOI: 10.1039/C8NJ01265B

variation is within a narrow range, this trend is consistent with electronic identities of the substituents.

Furthermore, lower emission quantum yields could be observed for the C2-symmetric ligand analogues in which both 1H-imidazole protons are unsubstituted (i.e. ligands **1** – **6**, Table 2). In particular, the very low quantum yield of compound **2** is remarkable and attractive for high turn-on intensity ratio; i.e. 'ligand+metal' emission (F) to 'ligand alone' emission (F_o). Conversely, the **7** and **10** – **13** ligand analogues possess higher quantum yields, which is unfavourable for high F/F_o values. Partial solubility prevented quantum yields estimations for **8** and **9**, but the emission intensities observed for the dissolved amounts suggests that they would also have appreciable quantum yields (Fig. 5 (c)). Large Stoke's shift values, which ranged from 113 – 168 nm, indicate ESIPT activity (Table 2,). This fact is confirmed by the lower Stoke's shift of 69 nm recorded for ligand **13**, which has no intramolecular hydrogen bonds (Fig. 5 (c) and Fig. 7 (a) inset (ii)).

It was concluded that the presence of several active protons (two from NH of imidazoles and one from phenolic OH) contributed to fluorescence weakening for the ligands that displayed low emissions (e.g. **1** – **6**). This conclusion may be explained by the thermal deactivation of fluorescence excited states by multiple fast proton exchange processes. On the other hand, possession of non-symmetrically substituted imidazoles (**10** – **12**), substitution of one or both 1H-imidazole protons (**7**, **9** – **11**) or presence of the fused aromatic phenanthreneyl moiety (**7** and **8**) appear to encourage higher quantum yields (see ligand-only emissions in Fig. 5 (b) and (c)). A lower Stock's shift of 69 nm and higher emission quantum yield recorded for compound **13**, which was deliberately included in this study for comparison and as a version of ligand **1** without the central hydroxyl function, respectively confirms the conclusions about importance of ESIPT

View Article Online
DOI: 10.1039/C8NJ01265B

activity and the role of hydrogen bonding relay to observed spectroscopic trends (Fig. 5 (c)). In other words, ligand **13** lacks the ability to make intramolecular donor-acceptor hydrogen bonds due to absence of the central hydroxyl function as possessed by the rest of the ligands. Consequently, absence of ESIPT process in compound **13** as revealed by lower Stoke's shift and the higher emission quantum yield, which is also consistent with absence of fast proton exchange processes, are not unexpected.

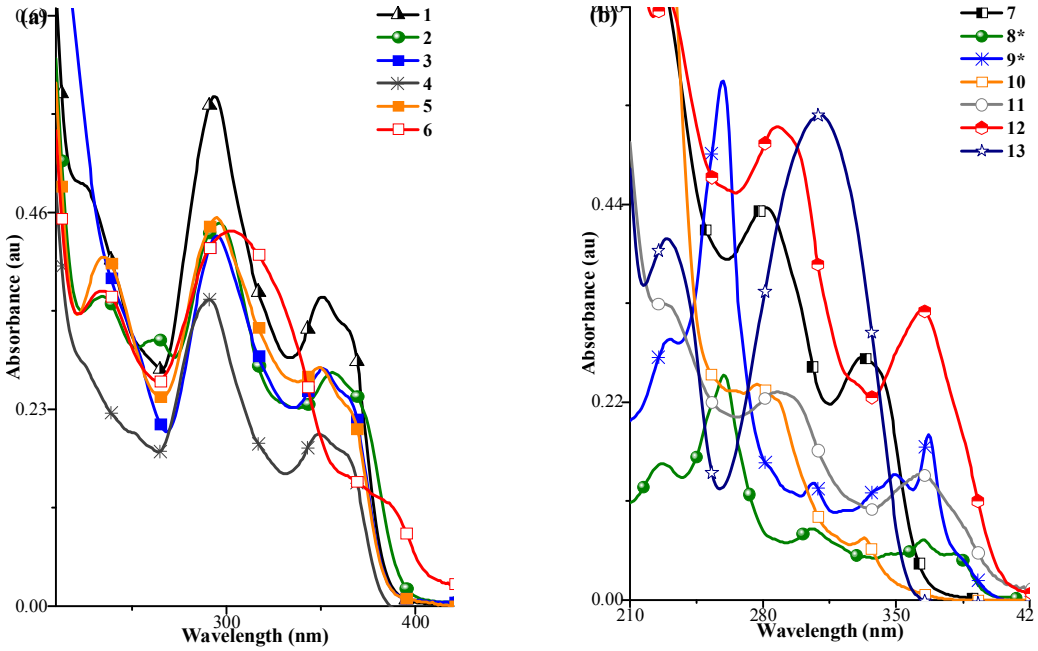

Fig. 4**:** Absorption spectra of the organic ligands in acetonitrile; (a) ligands **1** – **6**, (b) ligands **7** - **13**.

Table 2**:** Data for absorption and fluorescence features of the studied sensor candidates[a]

Compds.	$\lambda_{max(Abs)}$(nm)	$\lambda_{max(Ex)}$(nm)	$\lambda_{max(Em)}$(nm)	Stoke's Shift (nm)[d]	Φ
1	351, 293, 221[c]	360	492	132	0.026

View Article Online
DOI: 10.1039/C8NJ01265B

2	356, 296, 236	346	488	142	**0.007**
3	351, 295	350	491	141	0.035
4	349, 291	347	492	145	0.022
5	349, 294, 235	353	497	144	0.044
6	~365[c], 303, 235	332	504	172	0.072
7	332, 282	341	509	168	0.200
8[b]	379, 260, 228	364	498	134	[b]
9[b]	~367[c], 259	367	509	142	[b]
10	360, 294	355	522	167	0.081
11	363, 290, 224[c]	356	517	161	0.419
12	364, 288, 231	395	508	113	0.612
13	310, 230	332	401	69	0.232

[a]Solvent is acetonitrile and λ_{max} represent spectral peak positions; [b]Poor solubility in acetonitrile; [c]Appears as shoulder; [d]Stoke's shifts are the derived as the difference between excitation and emission peak positions.

3.4 Sensitivity of the ligands to metal ions

As a preamble, the F/F_o values for ligand **1** (i.e. ratio of photoluminescence intensity in the presence of metal ions to intensity in the absence) were measured for K^+, Ca^{2+}, Ba^{2+}, NH_4^+, Cr^{3+}, Mn^{2+}, Fe^{2+}, Co^{2+}, Ni^{2+}, Cu^{2+}, Zn^{2+}, Cd^{2+}, Ag^+ and Hg^{2+}. These preliminary F/F_o values indicated very high turn-on response for Cr^{3+} while Zn^{2+} and Cd^{2+} also appeared to yield a lower

View Article Online
DOI: 10.1039/C8NJ01265B

fluorescent turn-on. Therefore, further attentions for F/F_o evaluations were concentrated on Cr^{3+}, Zn^{2+} and Cd^{2+} for the purpose of comparing ligand performances within ligands **1** – **13**.

Consequently, F/F_o values for Cr^{3+} detection were determined for each of probes **1** – **13** and presented in Fig. 5 (a) as bar chart. High F/F_o values are recorded for ligands in which both imidazole rings bear the NH protons as well as same substituents on the 4,5-imidazole carbons (i.e. **1** – **6**) and their fluorescence turn-on signals follow the trend **2** (106 fold) >> **1** (23 fold) > **4** (19 fold) > **3** (17 fold) > **6** (8 fold) > **5** (7 fold). Compared to reported chromium(III) turn-on sensors, the over hundred-fold F/F_o signal by ligand **2** is highly remarkable (Scheme 1 (b)).[10,18–23]

It is however necessary to observe that the actual comparative details of turn-on behaviours is somewhat deemphasized by the F/F_o ratios. For instance, turn-on emission intensities for probes **1**, **3** and **4** are actually as well very strong, but the F/Fo values suggest they are only about one quarter as strong as for sensor probe **2**. Therefore, in order to make proper illustration of the turn-on strengths, efforts were made to also present various illustrational figures for the emission intensities of relevant experiments in this submission. For instance, the corresponding emission spectral stacks for Cr^{3+} detection experiments by ligands **1** – **13** are shown in Fig. 5 (b) and (c) while emission intensities in the presence (patterned bars) and absence (solid black bars) of Cr^{3+} is further presented as bar chart inset in Fig. 5 (a).

It is worthy of note that despite the metal-ligand interactions between Cr^{3+} and each of the ESIPT enabled probes **1** – **12**, the excitation and fluorescence emission peak positions for the 'Cr^{3+} + ligand' solutions remained generally at the same wavelengths as for the corresponding ligands. Therefore, it could be concluded that the resulting Cr^{3+}-ligand species formed are so

View Article Online
DOI: 10.1039/C8NJ01265B

configured that the ESIPT possibility is preserved as evidenced by the continued existence of large Stoke's shifts after addition of Cr^{3+}. This spectroscopic result is consistent with the one-pocket N^O chelation mode exemplified by the crystal structure of **7**-$CoCl_2$ (Fig. 2) so that the second N^O pocket still furnishes intramolecular hydrogen bond.

Considering Cd^{2+}, only about 10-fold emission increase was encountered for compounds **1**, **3** and **4** while about 30-fold turn-on was recorded for **2**. Furthermore, comparing among the ligands **1** – **13**, results show a very similar F/F_o trend as observed for Cr^{3+} except for the overall weaker turn-on intensities as well as absence of turn-on from ligand **6** (Fig. 6). Despite the weaker fluorescence response towards Cd^{2+}, this results provide a clue that further derivatization of the model sensor molecules may successfully deliver an applicable and powerful sensor candidate for Cd^{2+}. ESIPT character of the ligands were also preserved in the presence of Cd^{2+}, which suggests agreement with single pocket N^O coordination semblance of crystal structure **7**-$CoCl_2$ (Fig. 2).

The Zn^{2+} sensitivity results for ligands **1** – **11** are presented in Fig. 7 (a) and (b). A very attractive outcome of fluorescence hypsochromic shift to shorter wavelength was observed on addition of Zn^{2+} (Fig. 7 (a) inset (i)). Consequently, values of F/F_o in the Zn^{2+} detection experiment were derived at the blue-shifted response wavelengths and the greenish-to-blue fluorescence change can also be visibly observed (Fig. 9). While several members of the series displayed the hypsochromic spectral shift, only ligands **1** – **5**, **7** and **11** produced appreciable turn-on in addition to the spectral blue-shifts and the F/F_o signal is particularly impressive for ligand **1** (Fig. 7 (a)). It is also important to recognize that the hypsochromic shifts imply that fluorescent sensing of Zn^{2+} and Cr^{3+} would not interfere with each other and that the ESIPT feature of the ligands is lost in the presence of Zn^{2+}. Thus, the coordination interaction between

View Article Online
DOI: 10.1039/C8NJ01265B

the ligands and Zn^{2+} could be considered to frustrate further existence of intramolecular hydrogen bonding. This effect may probably be attributed to peculiarity of zinc-oxygen affinity and a resultant alteration of electronic character of the central oxy-atom of the ligands.

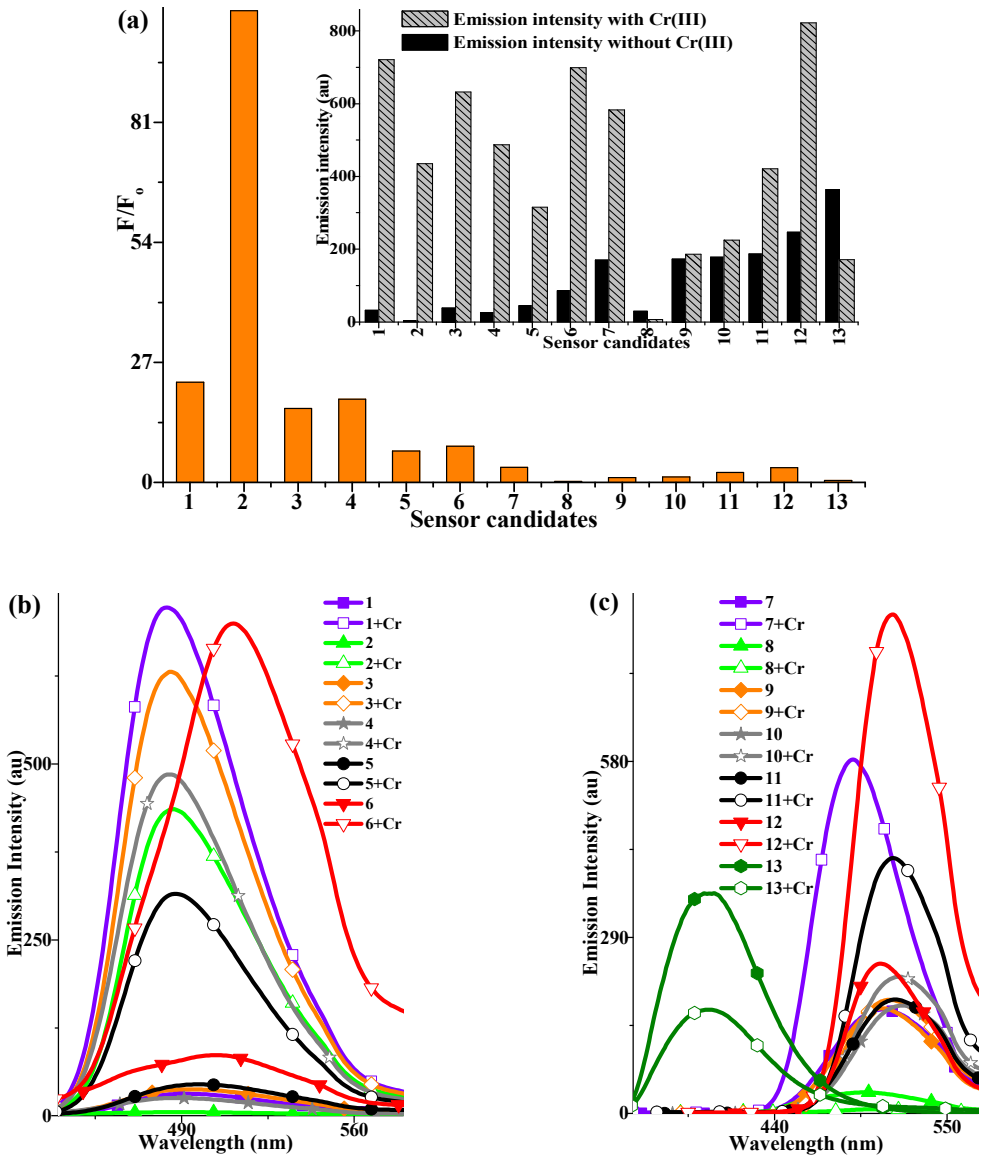

Fig. 5: (a) Results of Cr^{3+} sensitivity experiments as bar charts of F/F_o and inset comparing fluorescence intensities in the absence (black bars) and presence (patterned bars) of Cr^{3+} for

View Article Online
DOI: 10.1039/C8NJ01265B

ligands **1** – **13**; (b) emission spectra for ligands **1** – **6** in the absence and presence of Cr^{3+}; (c) emission spectra for ligands **7** – **13** in the absence and presence of Cr^{3+}

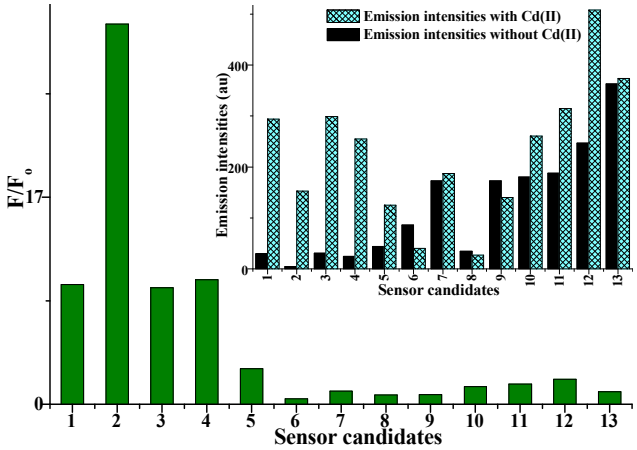

Fig. 6: Bar charts showing magnitudes of F/F_o for fluorescence changes due to Cd^{2+} interaction with ligands **1** to **13**. Inset shows comparison of actual emission intensity magnitudes for all the studied ligands in the absence (black) and presence (patterned) of Cd^{2+}.

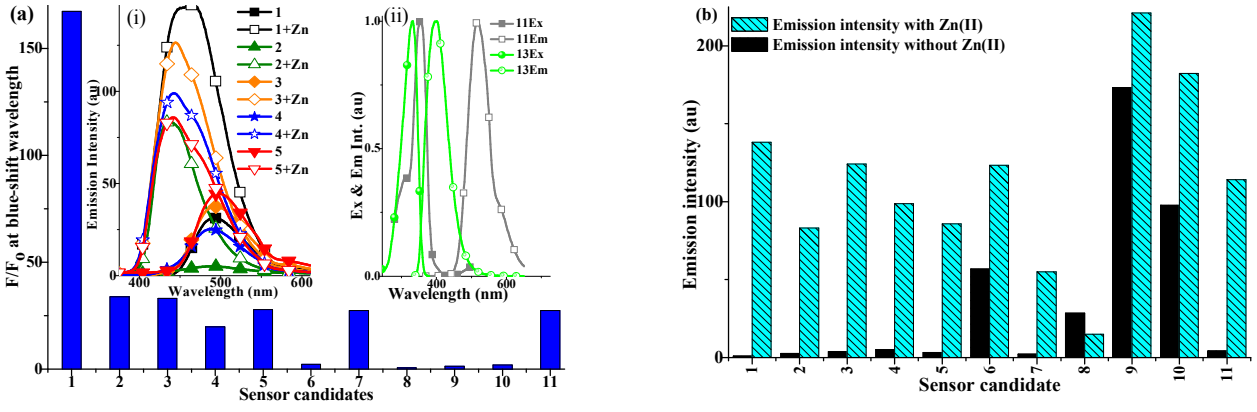

Fig. 7: (a) Bar charts showing magnitudes of F/F_o in Zn(II) sensitivity experiments with inset (i) showing blue-shifted turn-on spectra for ligands **1** – **5** and inset (ii) presenting normalized

View Article Online
DOI: 10.1039/C8NJ01265B

spectra illustrating the large Stoke's shift of ligand **11** against the small Stoke's shift of ligand **13**, (b) comparative emission intensity magnitudes for ligands **1** – **11** in the absence (black solid) and presence (patterned) of Zn(II)

3.5 Selectivity results

As can be concluded from the sensitivities tests, the 2,6-bis(4,5-diphenyl-1H-imidazol-2-yl)-4-methylphenol derivatives possess attractive sensor capabilities towards Cr^{3+} and Zn^{2+} while showing potentials for Cd^{2+}. To what extents are other commonly encountered cations able to produce interfering turn-on signals relative to values afforded by Cr^{3+}, Zn^{2+} and Cd^{2+}? Could there be any detectible molecular advantage resulting from substituent variations? In efforts to consider this aspects, ligand derivatives **1** – **4** were further subjected to selectivity tests. Therefore, fluorescent response (F/F_o) by each of probes **1** – **4** in the presence of K^+, Ca^{2+}, Ba^{2+}, NH_4^+, Cr^{3+}, Mn^{2+}, Fe^{2+}, Co^{2+}, Ni^{2+}, Cu^{2+}, Zn^{2+}, Cd^{2+}, Ag^+ and Hg^{2+} ions were obtained and compared.

Despite the iso-electronic characters of **1** – **4**, significant differences exist in their selectivity profiles in the presence of varying cations. Fig. 8 (a) compares the F/F_o values for the various cations with corresponding F/F_o for Cr^{3+} and Cd^{2+} as bar charts; $\boldsymbol{\lambda_{max(Em)}}$ ~485 nm, probe **1** (cross-line pattern), probe **2** (bars without patterns), probe **3** (horizontal-line pattern) and **4** (vertical-line pattern). Results for a similar comparative study for F/F_o of Zn^{2+} at its blue-shifted emission wavelengths are collected in Fig. 8 (b); $\boldsymbol{\lambda_{max(Em)}}$ ~440 nm, probe **1** (bars without pattern), probe **2** (horizontal-line pattern), probe **3** (cross-line pattern) and **4** (vertical-line pattern).

View Article Online
DOI: 10.1039/C8NJ01265B

For ligand **1**, Fe^{2+}, Co^{2+} and Cd^{2+} also caused up to 30 % of the impressive 25-fold fluorescence turn-on enabled by Cr^{3+}; i.e. 13-, 9- and 10-folds respectively. Therefore, these three metal ions could weaken the selectivity prospect of ligand **1** as Cr^{3+} sensor. On the other hand, none of the other cations possessed up to 30 % of the very high fluorescence turn-on achieved by compound **2** as Cr^{3+} sensor. The nearest to 30 % of the 106-fold Cr^{3+} sensing response is afforded by Cd^{2+}. Despite the about 20 % of Cr^{3+}'s F/F_o values also measured for K^+, Ca^{2+} and Mn^{2+}, the performance of ligand **2** as Cr^{3+} sensor strongly stands out and surpasses interferences (Fig. 8 (a) and inset (i) of Fig. 8 (b)). Also considering the Cr^{3+} turn-on by ligands **3** (F/F_o = 18) and **4** (F/F_o = 25), only Cd^{2+} showed up to 30 % competitive response, which is then followed by Co^{2+} (Fig. 8 (a) and inset (ii) of Fig. 8 (b)).

Similar evaluation on ligands **1** – **4** for Zn^{2+} selectivity at the blue-shift emission wavelengths (438 nm – 450 nm) show that ligands **1**, **3** and **4** demonstrated good selectivity results, which is disallowed by K^+ and Ca^{2+} in the case of **2**. The outcome is quite remarkable in the cases of **1** (Fig. 8 (b)).

It could therefore be concluded that the mild substituent variations could be employed to exclude interferences from various ions. One example of observable derivatization effect is that, while Co^{2+} may play weak interference role in Cr^{3+} detection by probe candidates **1**, **3** and **4**, this undesirable effect is totally obliterated for ligand **2**. Furthermore, observing the cation-ligand solutions under a 365 nm UV lamp (Fig. 9), it is noteworthy that even the 25-fold turn-on for ligand **4** is already efficient enough to demonstrate the attractive sensitivity and selectivity for Cr^{3+} by these probes.

View Article Online
DOI: 10.1039/C8NJ01265B

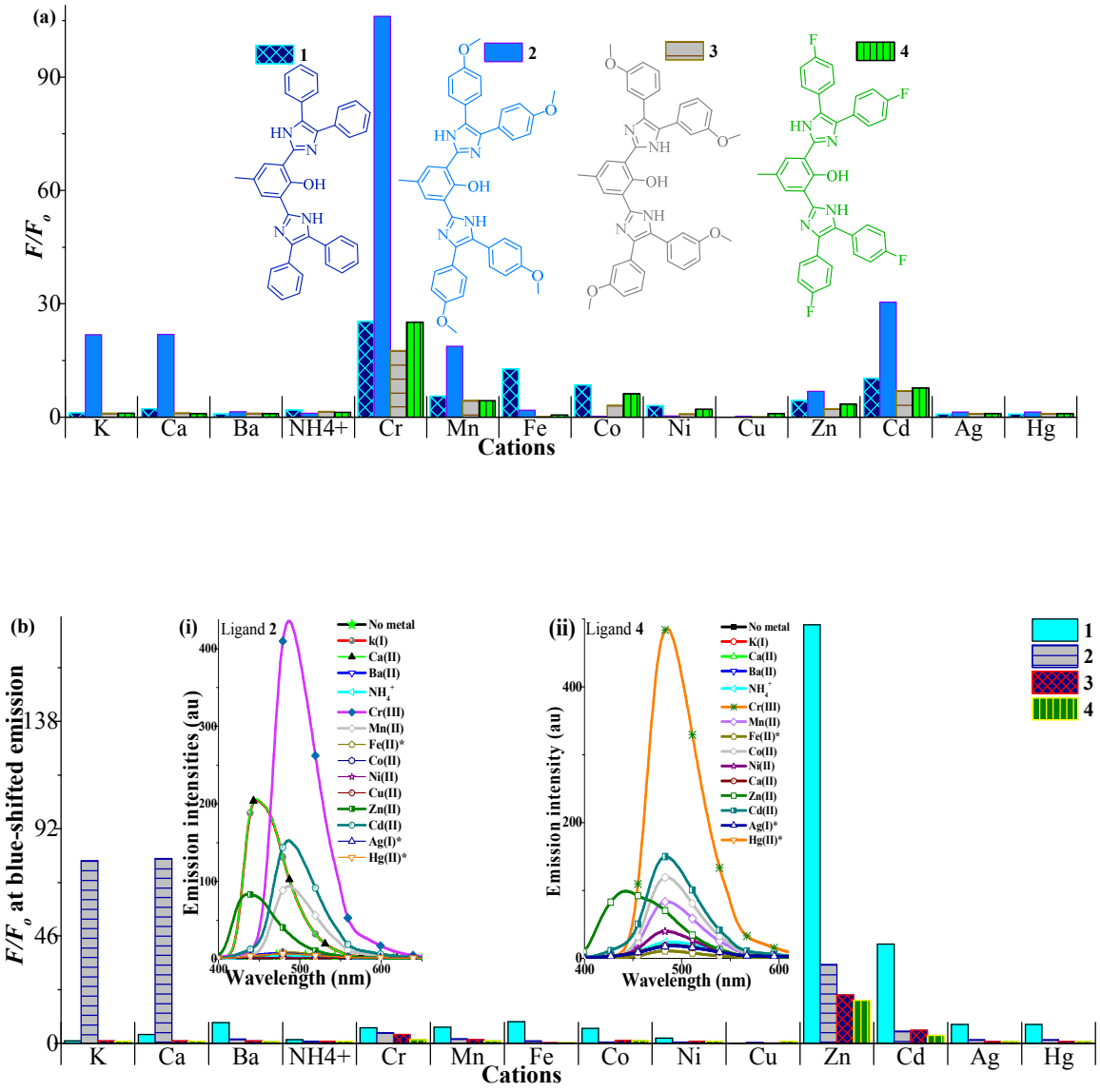

Fig. 8: Bar charts comparing F/F_o values in the presence of various cations for probes **1** – **4**: (a) Shows extents of turn-on from other cations alongside Cr^{3+} and Cd^{2+}at ~485 nm; (b) Shows extents of turn-on from other cations alongside Zn^{2+} at ~440 nm while insets (i) and (ii) present the strong selectivity for Cr^{2+} as well as blue shifted Zn^{2+} emission turn-on

View Article Online
DOI: 10.1039/C8NJ01265B

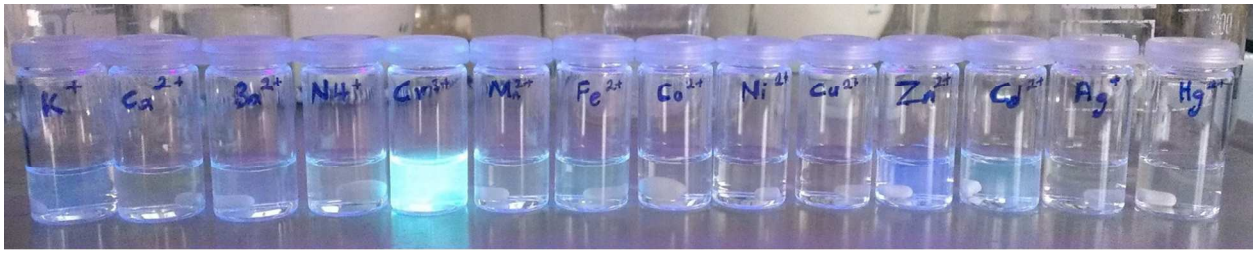

Fig. 9: Fluorescence of **4** in the presence of various cations showing visible sensor strength for Cr^{3+} and the weakness of interference from other cations (note that some brightness seen in vial near the Cr^{3+}vial come from the Cr^{3+} vial)

3.6 Varying concentrations, Job plot and acid/base

Titration experiment of Cr^{3+} against ligand **3** reveals linear fluorescence increase till one equivalent of Cr^{3+} has been added. Further addition of Cr^{3+} results in gradually reducing emission intensity (Fig. 10 (a)). Job plots obtained for ligand **4** against Cr^{3+} (Fig. 10 (b)) or Zn^{2+} (Fig. 10 (c)) indicates that the fluorescent species responsible for turn-on emissions are assembled in 1:1 mole ratio. Therefore, a one pocket N^O 1:1 coordination similar to the observed single crystal result (Fig. 1) is proposed as the effective interaction leading to the sensing action for Cr^{3+} and Cd^{2+} since the sustained ESIPT character in the presence of the metal ions also agrees with existence of a vacant, hydrogen bonded N^O pocket. On the other hand, Zn^{2+} caused loss of ESIPT and may not be according to the one-pocket N^O coordination. Finally, the presence of acid (weak or strong) turned on fluorescence of ligand **2** without blue-shifts while alkalinity maintains the ligand status quo (Fig. 10 (d)).

View Article Online
DOI: 10.1039/C8NJ01265B

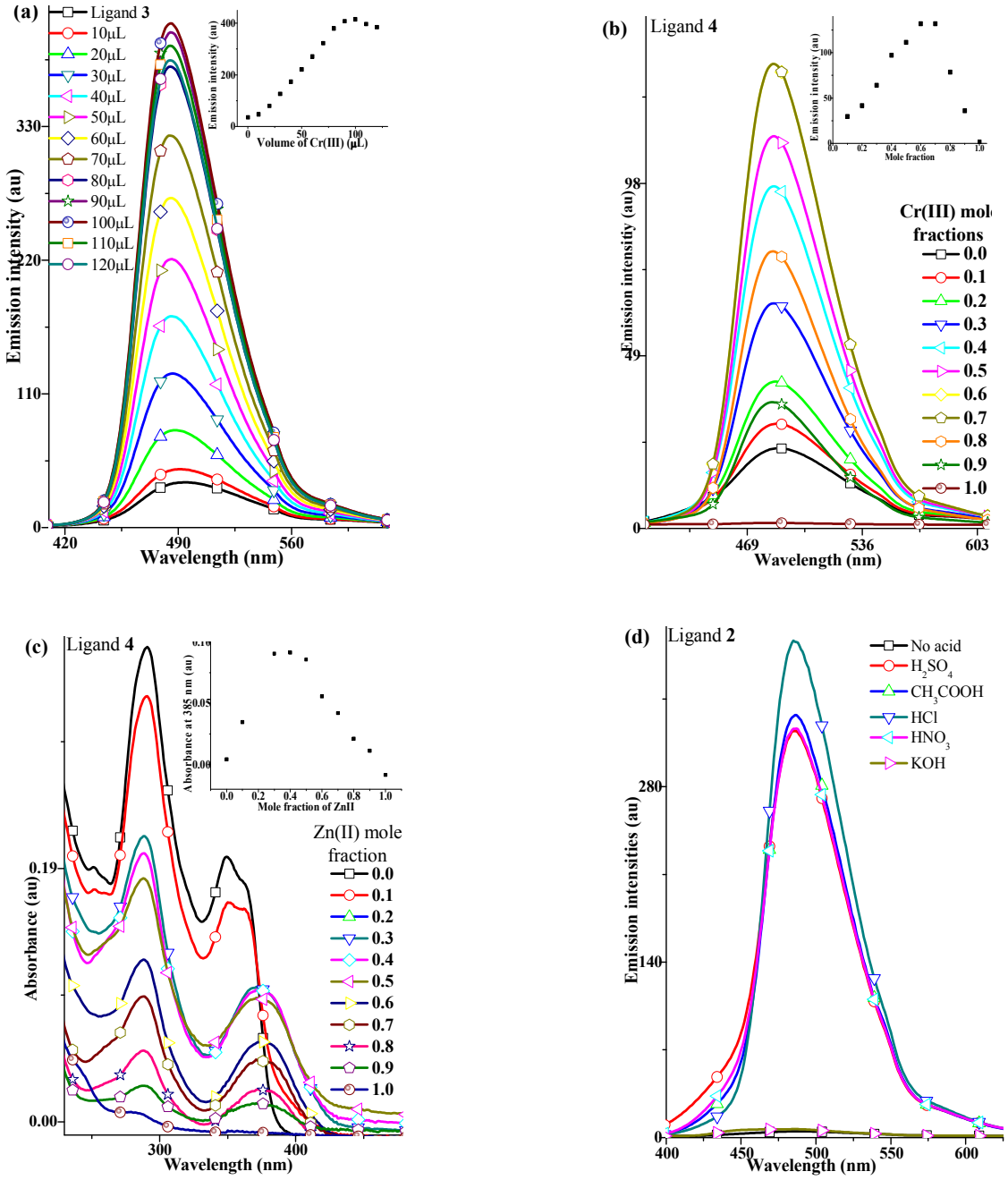

Fig. 10: (a) Cr^{3+} titration on **3**, (b) stacked emission spectra of **4** in the presence of Cr^{3+} mole fraction in the range 0 – 1, and (c) stacked absorption spectra of **4** in the presence of Zn^{2+} mole fraction in the range 0 – 1, (d) ligand **2** in the presence of acids and a base

View Article Online
DOI: 10.1039/C8NJ01265B

3.7 Theoretical Studies

To gain a qualitative insight into the photophysical origin of fluorescence turn-on due to Cr^{3+} coordination, second order multireference perturbation theoretical (MRPT2) calculations with various active space sizes and time-dependent density functional (TD-DFT/B3LYP) calculations were carried out using the model structures 1L, 2L, 1L-Cr^{3+} and 2LR (Fig. 11, see supporting information for calculation details). Calculations showed that the electronic ground states of 2-imidazolyl-phenol (model structure 1L), and 2,6-di(imidazolyl)-phenol (model structures 2L, 2LR) are spin singlets while that of Cr^{3+} coordinated 2-imidazolyl-phenol (model structure 1L-Cr^{3+}) is a spin quartet.

Measured absorption spectra of synthesized compounds **1** – **6** showed two absorbance maxima in the ranges 293 – 303 nm and 349 – 365 nm (Table 2 and Fig 4 (a)). Calculated values for the model structure 1L show only the first band, while those for 2L exhibit both. The first of these absorbance values is calculationally assigned to be ($1A' \leftarrow 0A'$) transition at positions 307, 301, 301 and 313 nm as calculated using TD-B3LYP, MRPT2(10,10), MRPT2(12,11), and MRPT(14,12) methods respectively. This agrees with reported experimental values for species containing 1L functionality.[27,40] The configuration interaction (CI) weights of the most dominant electronic configuration in multiconfigurational wavefunctions showed that ($1A' \leftarrow 0A'$) arises from $\pi\pi^*$ electronic excitations (Supplementary Information, Table S2).

The TD-B3LYP calculation for 2L reproduces both absorbance maxima of the synthesized compounds **1** – **6**, at 356 and 298 nm. Examination of Kohn-Sham orbitals involved in these transitions revealed that the second of the two maxima matches with above mentioned 1L absorbance arising from $\pi\pi^*$ transition involving intramolecular hydrogen

View Article Online
DOI: 10.1039/C8NJ01265B

bonded imidazolyl-phenol moiety whereas the first of the two involves a different $\pi\pi^*$ transition centered on imidazolyl-phenol moiety formed with additional imidazole ring of 2L. An orthogonal orientation of the additional imidazole ring (Fig. 11) shifts these twin TD-B3LYP transitions respectively to close lying 322 and 312 nm spectral positions, suggesting that loss of planarity of the additional imidazole ring tends to merge two distinct bands and 2L appears to behave like 1L.

Given the excitation wavelength (λ_{ex}) employed in current work (332 – 360 nm) to study the emission behavior of ligands **1** – **6**, and their emission range (492 – 505), the fluorescent behavior of ligands arises from co-planar imidazole-phenolic-imidazole structures. Additionally, preserving of such co-planarity also guarantees the presence of low-lying electronic states involving excited state proton transfer.

The essential features of coordination of the analyte (Cr^{3+}) to synthesized ligands **1** – **6** are captured in model structure 1L-Cr^{3+}. Calculated CAS, ORMAS, and MRPT2 vertical excitation energies of 1L-Cr^{3+} show a prominent red shift in comparison to 1L (Supplementary Information, Table S3). Of the various electron active spaces and methods employed, the calculation with the largest active space involving inclusion of dynamic correlation energy is denoted MRPT2(15,13). The three lowest vertical excitation wavelength of 1L- Cr^{3+} at this level are 403, 356, and 338 nm compared to 313, 255, and 215 nm for 1L/MRPT2(14,12). The dominant contribution to electronic states (including electronic ground state) of 1L-Cr^{3+} arises from configurations having either three or five unpaired electrons variously occupying organic π, π^*, or three metal *d*-orbitals to form spin qurtets. The above mentioned red shifts on Cr^{3+} coordination are due to inclusion of various πd, $d\pi^*$ electronic configurations in

View Article Online
DOI: 10.1039/C8NJ01265B

multiconfigurational wave functions, in addition to pure π, and $\pi\pi^*$ configurations (Fig 12 and Supplementary Information, Table S2). It is obvious that narrowing of energy gap between ground and low lying excited states of 1L-Cr^{3+} guarantees availability of additional excited states populated by irradiation at λ_{ex}. Furthermore, the coordination of analyte restrict the free rotation of at least one imidazole ring with enforcing of ligand co-planarity. These factors may be crucial for enhanced emission quantum yields and fluorescent turn-on behaviour.

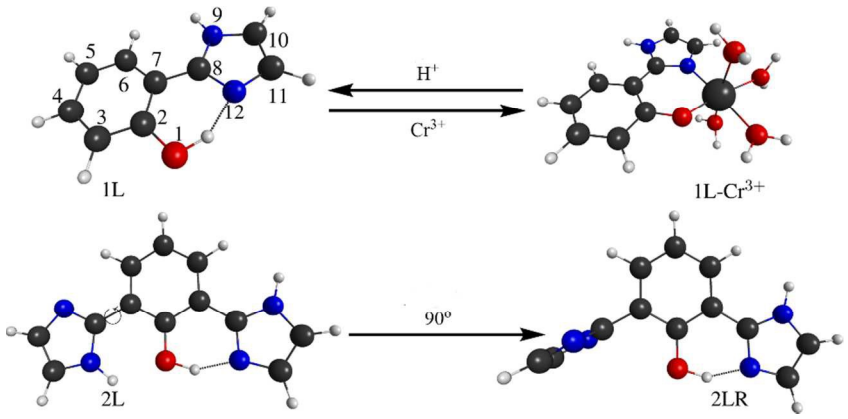

Fig. 11: Model structures utilized for theoretical calculations and optimized with def2-SV(P)/B3LYP

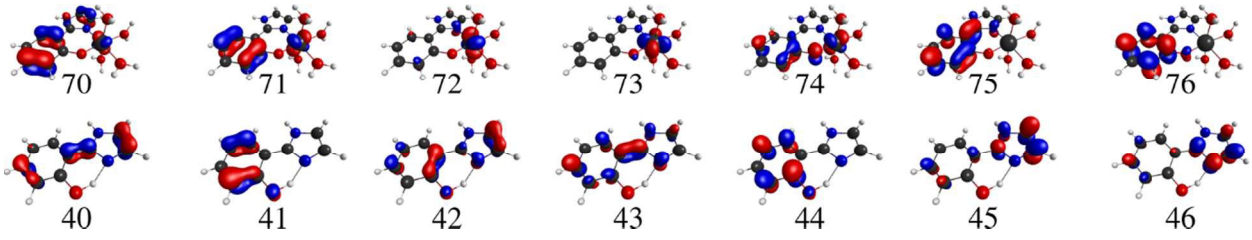

Fig. 12: Important state-averaged active orbitals from CAS(14,12) for 1L and ORMAS(17,14) for

View Article Online
DOI: 10.1039/C8NJ01265B

773 1L-Cr^{3+}

774

775 **4. Conclusion**

776 A series of ESIPT-capable 2,6-di(1H-imidazol-2-yl)phenol dyes (**1** – **12**) and an ESIPT-
777 incapable 1,3-bis(4,5-diphenyl-1H-imidazol-2-yl)benzene (**13**) were prepared and studied for
778 fluorescent sensing properties of metal ions. Single crystal structural results confirmed the
779 identity of as well as presence of anticipated hydrogen bond relay in the bi-imidazole-phenol
780 compounds. X-ray structures also revealed various possible metal coordination modes for the
781 studied ligands.

782 UV-vis and fluorescence spectral results showed that, while the electronic and
783 spectroscopic properties of the compounds depend largely on the protonation and substitution
784 situations directly on the 2,6-di(1H-imidazol-2-yl)-4-methylphenol nucleus, possibility exists to
785 derivatize and manipulate the molecules at other peripheral positions without perturbation of the
786 electronic properties of the nucleus (e.g. on 4,5-dipheny-imidazole rings as on **1** – **6**).

787 Furthermore, compounds **1** – **4** are presented in this submission as very sensitive and
788 selective Cr^{3+} fluorescent sensors with as high as 106-fold emission turn-on recorded for
789 molecule **2**. To the best of our knowledge, this magnitude of emission turn-on is unknown for
790 Cr^{3+}. Additionally, ligands **1** and **4** also show an interesting sensitivity and selectivity for Zn^{2+} at
791 a blue-shifted emission bands, which is remarkably exploitable in the case of ligand **1**. Results
792 revealed that Cd^{2+} sensor may be developed by further study of these probes. Presence of
793 multiple active protons involved in hydrogen bonding relay (i.e. from the phenol OH and the 1H-

View Article Online
DOI: 10.1039/C8NJ01265B

imidazole protons) in addition to symmetrical substitution of both imidazole rings (i.e. as for probes **1** – **6**) are key to desirable outcomes.

Based on Job plot, single crystal result and sustained ESIPT in turn-on emissions, a one pocket N^O coordination in 1:1 stoichiometry is proposed as the metal-ligand interactions responsible for the sensing actions. A key conclusion is that deliberate molecular derivatization can serve as a tool for understanding, tuning or improving selectivity and other desirable properties of chemosensors, which is not commonly encountered in molecular sensing reports. Therefore, avoidance of commonly encountered interferences in fluorescent sensing or design of sensors targeting certain two or more analyte metal ions may be achieved by careful derivatization. DFT calculations suggest that successful turn-on results may be associated with coplanarity settings of the imidazole and phenol rings in the presence and absence of the respective analyte metal ions.

Supplementary material

Crystallographic data (excluding structure factors) has been deposited with the Cambridge Crystallographic Data Centre as supplementary publication: CCDC-1505094 for **12** and CCDC-1505093 for **7**-$CoCl_2$. Copies of the data can be obtained free of charge on application to CCDC, 12 Union Road, Cambridge CB2 1EZ, UK [E- mail: deposit@ccdc.cam.ac.uk].

Acknowledgement

View Article Online
DOI: 10.1039/C8NJ01265B

A.O.E is grateful to the Alexander von Humboldt Foundation for postdoctoral research award that supported this project and to Redeemer's University for allowing fellowship leave. The authors thankfully acknowledge the use of the Computation café of Friedrich-Schiller Universität Jena. The financial support by the Deutsche Forschungsgemeinschaft (DFG) is gratefully acknowledged (PL 155/11, PL 155/12 and PL155/13).

References

1 H. N. Kim, W. X. Ren, J. S. Kim and J. Yoon, *Chemical Society reviews*, 2012, **41**, 3210–3244.
2 K. P. Carter, A. M. Young and A. E. Palmer, *Chemical reviews*, 2014, **114**, 4564–4601.
3 a) H. Zhu, J. Fan, B. Wang and X. Peng, *Chemical Society reviews*, 2015, **44**, 4337–4366; b) B. Kaur, N. Kaur and S. Kumar, *Coordination Chemistry Reviews*, 2018, **358**, 13–69;
4 S. Pal, N. Chatterjee and P. K. Bharadwaj, *RSC Adv.*, 2014, **4**, 26585.
5 a) Y. Li, F. Wei, Y. Lu, S. He, L. Zhao and X. Zeng, *Dyes and Pigments*, 2013, **96**, 424–429; b) J. J. Gooding, E. Bakker and S. Kelley, *ACS Sens.*, 2016, **1**, 324–325;
6 a) V. K. Gupta, A. K. Jain, P. Kumar, S. Agarwal and G. Maheshwari, *Sensors and Actuators B: Chemical*, 2006, **113**, 182–186; b) P. Joshi, M. Nair and D. Kumar, *Anal. Methods*, 2016, **8**, 1359–1366; c) H. A. Zamani, G. Rajabzadeh and M. R. Ganjali, *Sensors and Actuators B: Chemical*, 2006, **119**, 41–46; d) M. Rong, L. Lin, X. Song, Y. Wang, Y. Zhong, J. Yan, Y. Feng, X. Zeng and X. Chen, *Biosensors & bioelectronics*, 2015, **68**, 210–217; e) Juewen Liu and Yi Lu, *J. AM. CHEM. SOC.*, 2007, **129**, 9838–9839;
7 a) Y. Tan, J. Gao, J. Yu, Z. Wang, Y. Cui, Y. Yang and G. Qian, *Dalton transactions (Cambridge, England : 2003)*, 2013, **42**, 11465–11470; b) Y. W. Choi, G. R. You, J. J. Lee and C. Kim, *Inorganic Chemistry Communications*, 2016, **63**, 35–38;
8 a) E. J. Song, J. Kang, G. R. You, G. J. Park, Y. Kim, S.-J. Kim, C. Kim and R. G. Harrison, *Dalton transactions (Cambridge, England : 2003)*, 2013, **42**, 15514–15520; b) K. Aich, S. Goswami, S. Das, C. D. Mukhopadhyay, C. K. Quah and H.-K. Fun, *Inorganic chemistry*, 2015, **54**, 7309–7315;
9 N. Singla, A. Tripathi, M. Rana, S. Kishore Goswami, A. Pathak and P. Chowdhury, *Journal of Luminescence*, 2015, **165**, 46–55.
10 G. Balamurugan and S. Velmathi, *Photochemical & photobiological sciences : Official journal of the European Photochemistry Association and the European Society for Photobiology*, 2018, **17**, 239–244.
11 a) P. Tyagi, S. Chandra and B. S. Saraswat, *Spectrochimica acta. Part A, Molecular and biomolecular spectroscopy*, 2015, **134**, 200–209; b) P. Naveen, R. Jain, P. Kalaivani, R. Shankar, F. Dallemer and R. Prabhakaran, *New J. Chem.*, 2017, **41**, 8885–8898;

View Article Online
DOI: 10.1039/C8NJ01265B

12 a) L. Xu, M.-L. He, H.-B. Yang and X. Qian, *Dalton transactions (Cambridge, England : 2003)*, 2013, **42**, 8218–8222; b) Q. Zhao, R.-F. Li, S.-K. Xing, X.-M. Liu, T.-L. Hu and X.-H. Bu, *Inorganic chemistry*, 2011, **50**, 10041–10046;

13 a) R. Ali, S. M. Saleh and R. F. M. Elshaarawy, *RSC Adv.*, 2016, **6**, 86965–86975; b) N. Suzuki, K. Suda, D. Yokogawa, H. Kitoh-Nishioka, S. Irle, A. Ando, L. M. G. Abegão, K. Kamada, A. Fukazawa and S. Yamaguchi, *Chem. Sci.*, 2018, **9**, 2666–2673;

14 Y. Jiao, B. Zhu, J. Chen and X. Duan, *Theranostics*, 2015, **5**, 173–187.

15 a) A. Zhitkovich, *Chemical research in toxicology*, 2011, **24**, 1617–1629; b) A. K. Shanker, C. Cervantes, H. Loza-Tavera and S. Avudainayagam, *Environment international*, 2005, **31**, 739–753;

16 a) J. B. Vincent, *Dalton transactions (Cambridge, England : 2003)*, 2010, **39**, 3787–3794; b) K. R. Di Bona, S. Love, N. R. Rhodes, D. McAdory, S. H. Sinha, N. Kern, J. Kent, J. Strickland, A. Wilson, J. Beaird, J. Ramage, J. F. Rasco and J. B. Vincent, *Journal of biological inorganic chemistry : JBIC : a publication of the Society of Biological Inorganic Chemistry*, 2011, **16**, 381–390; c) J. Zhao, L. Xia, A. Sehgal, D. Lu, R. L. McCreery and G. S. Frankel, *Surface and Coatings Technology*, 2001, **140**, 51–57;

17 a) K. Rajendran, S. Manikandan, L. D. Nair, R. Karuthodiyil, N. Vijayarajan, R. Gnanasekar, V. V. Kapil and A. S. Mohamed, *Journal of clinical and diagnostic research : JCDR*, 2015, **9**, OC05-8; b) S. K. Panda, *Journal of plant physiology*, 2007, **164**, 1419–1428; c) R. Bencheikh-Latmani, A. Obraztsova, M. R. Mackey, M. H. Ellisman and B. M. Tebo, *Environ. Sci. Technol.*, 2007, **41**, 214–220;

18 X. Hu, J. Chai, Y. Liu, B. Liu and B. Yang, *Spectrochimica acta. Part A, Molecular and biomolecular spectroscopy*, 2016, **153**, 505–509.

19 C. Fan, X. Huang, C. A. Black, X. Shen, J. Qi, Y. Yi, Z. Lu, Y. Nie and G. Sun, *RSC Adv*, 2015, **5**, 70302–70308.

20 Z. Zhou, M. Yu, H. Yang, K. Huang, F. Li, T. Yi and C. Huang, *Chemical communications (Cambridge, England)*, 2008, 3387–3389.

21 X.-M. Li, R.-R. Zhao, Y. Yang, X. W. Lv, Y.-L. Wei, R. Tan, J.-F. Zhang and Y. Zhou, *Chinese Chemical Letters*, 2017, **28**, 1258–1261.

22 A. N. Kursunlu, E. Şahin and E. Güler, *RSC Adv.*, 2015, **5**, 5951–5957.

23 M. Zhao, L. Ma, M. Zhang, W. Cao, L. Yang and L.-J. Ma, *Spectrochimica acta. Part A, Molecular and biomolecular spectroscopy*, 2013, **116**, 460–465.

24 Y. Zhou, Z.-X. Li, S.-Q. Zang, Y.-Y. Zhu, H.-Y. Zhang, H.-W. Hou and T. C. W. Mak, *Organic letters*, 2012, **14**, 1214–1217.

25 H. Wu, Q. Liao, S. N. Chillrud, Q. Yang, L. Huang, J. Bi and B. Yan, *Scientific reports*, 2016, **6**, 29989.

26 A. O. Eseola, O. Adepitan, H. Görls and W. Plass, *New J. Chem.*, 2012, **36**, 891.

27 A. O. Eseola, W. Li, R. Gao, M. Zhang, X. Hao, T. Liang, N. O. Obi-Egbedi and W.-H. Sun, *Inorganic chemistry*, 2009, **48**, 9133–9146.

28 a) A. O. Eseola, D. Geibig, H. Görls, W.-H. Sun, X. Hao, J. A. O. Woods and W. Plass, *Journal of Organometallic Chemistry*, 2014, **754**, 39–50; b) A. O. Eseola, W. Li, W.-H. Sun, M. Zhang, L. Xiao and J. A.O. Woods, *Dyes and Pigments*, 2011, **88**, 262–273; c) A. O. Eseola, W. Li, O. G. Adeyemi, N. O. Obi-Egbedi and J. A.O. Woods, *Polyhedron*, 2010, **29**, 1891–1901; d) A. O. Eseola, W.-H. Sun, W. Li and J. A.O. Woods, *Journal of Molecular Structure*, 2010, **984**, 117–124;

29 A. O. Eseola, O. Akogun, H. Görls, O. Atolani, G. A. Kolawole and W. Plass, *Journal of Molecular Catalysis A: Chemical*, 2014, **387**, 112–122.

View Article Online
DOI: 10.1039/C8NJ01265B

30 A. O. Eseola, H. Görls, J. A.O. Woods and W. Plass, *Journal of Molecular Catalysis A: Chemical*, 2015, **406**, 224–237.

31 a) *COLLECT, Data Collection Software; Nonius B.V., Netherlands, 1998.*; b) Z. Otwinowski and W. Minor, in *Macromolecular crystallography*, ed. C. W. Carter and R. M. Sweet, Elsevier Academic Press, Amsterdam, London, 1997-, vol. 276, pp. 307–326; c) *SADABS 2.10, Bruker-AXS inc., 2002, Madison, WI, U.S.A.*;

32 G. M. Sheldrick, *Acta crystallographica. Section A, Foundations of crystallography*, 2008, **64**, 112–122.

33 *XP; Siemens Analytical X-ray Instruments Inc.: Karlsruhe, Germany, 1990; Madison, WI, USA, 1994.*

34 A. M. Brouwer, *Pure and Applied Chemistry*, 2011, **83**, 2213–2228.

35 J. S. Renny, L. L. Tomasevich, E. H. Tallmadge and D. B. Collum, *Angewandte Chemie (International ed. in English)*, 2013, **52**, 11998–12013.

36 University of Karlsruhe and Forschungszentrum Karlsruhe GmbH, 1989 - 2007, *TURBOMOLE V7.1 2016,* available at: available from http://www.turbomole.com.

37 a) K. Hirao, *Chemical Physics Letters*, 1992, **190**, 374–380; b) K. Hirao, *Chemical Physics Letters*, 1992, **196**, 397–403; c) K. Hirao, *Chemical Physics Letters*, 1993, **201**, 59–66; d) K. Hirao, *Int. J. Quantum Chem.*, 1992, **44**, 517–526;

38 M. W. Schmidt, K. K. Baldridge, J. A. Boatz, S. T. Elbert, M. S. Gordon, J. H. Jensen, S. Koseki, N. Matsunaga, K. A. Nguyen, S. Su, T. L. Windus, M. Dupuis and J. A. Montgomery, *J. Comput. Chem.*, 1993, **14**, 1347–1363.

39 J. G. Lombardino and E. H. Wiseman, *J. Med. Chem.*, 1974, **17**, 1182–1188.

40 a) L. Benisvy, A. J. Blake, D. Collison, E. Stephen Davies, C. David Garner, E. J. L. McInnes, J. McMaster, G. Whittaker and C. Wilson, *Dalton Trans*, 2003, **vol. 30**, 1975–1985; b) M. Bräuer, M. Mosquera, J. L. Pérez-Lustres and F. Rodríguez-Prieto, *J. Phys. Chem. A*, 1998, **102**, 10736–10745; c) L. Benisvy, A. J. Blake, E. S. Davies, C. D. Garner, J. McMaster, C. Wilson, D. Collison, E. J. L. McInnes and G. Whittaker, *Chem. Commun.*, 2001, 1824–1825;

View Article Online
DOI: 10.1039/C8NJ01265B

ESIPT-capable 2,6-di(1H-imidazol-2-yl)phenols with very strong fluorescent sensing signals towards Cr(III), Zn(II) and Cd(II): molecular variation effects on turn-on efficiency

Abiodun O. Eseola,[§,‡,*] Helmar Görls,[‡] Masroor Bangesh,[†] Winfried Plass,[‡,*]

[§]Materials Chemistry group, Department of Chemical Sciences, Redeemer's University Ede, Osun State, Nigeria.

[‡]Institut für Anorganische und Analytische Chemie, Friedrich-Schiller-Universität Jena, Humboldtstr. 8, D-07743 Jena, Germany.

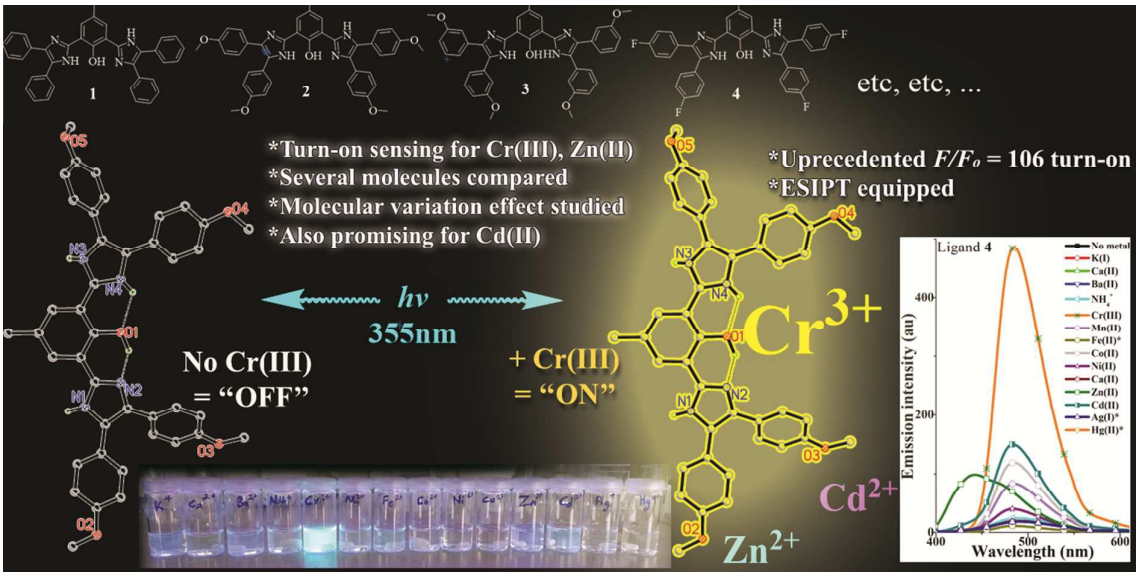

Derivatization influence was studied for twelve 2,6-di(1H-imidazol-2-yl)phenols, strong fluorescent sensitivity for Cr(III) is reported while Zn(II)/Cd(II) sensing potentials also appeared.

* Corresponding authors: Dr. A. O. Eseola: Materials Chemistry group, Department of Chemical Sciences, Redeemer's University Ede, Osun State, Nigeria; Tel.: +49(0)15218016407, +493641948138. e-mail: bioduneseola@hotmail.com; biodun.eseola@uni-jena.de; Prof. Dr. W. Plass; Address – Institut für Anorganische und Analytische Chemie, Friedrich-Schiller-Universität Jena, Humboldtstr. 8, D-07743 Jena, Germany; Tel.: +49 3641 948130; Fax: +49 3641948132; e-mail: sekr.plass@uni-jena.de

Electronic Supplementary Information (ESI) containing some further details is provided.